




ORIGINAL PAPER

Open Access



Urban cooling potential and cost comparison of heat mitigation techniques for their impact on the lower atmosphere

Ansar Khan¹, Laura Carlosena^{2*} , Samiran Khorat³, Rupali Khatun³, Debashish Das⁴, Quang-Van Doan⁵, Rafiq Hamdi⁶, Sk Mohammad Aziz⁷, Hashem Akbari⁸, Mattheos Santamouris⁹ and Dev Niyogi¹⁰

Abstract

Cool materials and rooftop vegetation help achieve urban heating mitigation as they can reduce building cooling demands. This study assesses the cooling potential of different mitigation technologies using Weather Research and Forecasting (WRF)- taking case of a tropical coastal climate in the Kolkata Metropolitan Area. The model was validated using data from six meteorological sites. The cooling potential of eight mitigation scenarios was evaluated for: three cool roofs, four green roofs, and their combination (cool-city). The sensible heat, latent heat, heat storage, 2-m ambient temperature, surface temperature, air temperature, roof temperature, and urban canopy temperature was calculated. The effects on the urban boundary layer were also investigated.

The different scenarios reduced the daytime temperature of various urban components, and the effect varied nearly linearly with increasing albedo and green roof fractions. For example, the maximum ambient temperature decreased by 3.6 °C, 0.9 °C, and 1.4 °C for a cool roof with 85% albedo, 100% rooftop vegetation, and their combination.

The cost of different mitigation scenarios was assumed to depend on the construction options, location, and market prices. The potential for price per square meter and corresponding temperature decreased was related to one another. Recognizing the complex relationship between scenarios and construction options, the reduction in the maximum and minimum temperature across different cool and green roof cases were used for developing the cost estimates. This estimate thus attempted a summary of the price per degree of cooling for the different potential technologies.

Higher green fraction, cool materials, and their combination generally reduced winds and enhanced buoyancy. The surface changes alter the lower atmospheric dynamics such as low-level vertical mixing and a shallower boundary layer and weakened horizontal convective rolls during afternoon hours. Although cool materials offer the highest temperature reductions, the cooling resulting from its combination and a green roof strategy could mitigate or reverse the summertime heat island effect. The results highlight the possibilities for heat mitigation and offer insight into the different strategies and costs for mitigating the urban heating and cooling demands.

Keywords Urban heating, Cool roofs, Green roofs, Cool city, WRF/SLUCM, Building cooling demand

*Correspondence:

Laura Carlosena
laura.carlosena@unavarra.es

Full list of author information is available at the end of the article



© The Author(s) 2023. **Open Access** This article is licensed under a Creative Commons Attribution 4.0 International License, which permits use, sharing, adaptation, distribution and reproduction in any medium or format, as long as you give appropriate credit to the original author(s) and the source, provide a link to the Creative Commons licence, and indicate if changes were made. The images or other third party material in this article are included in the article's Creative Commons licence, unless indicated otherwise in a credit line to the material. If material is not included in the article's Creative Commons licence and your intended use is not permitted by statutory regulation or exceeds the permitted use, you will need to obtain permission directly from the copyright holder. To view a copy of this licence, visit <http://creativecommons.org/licenses/by/4.0/>.

1 Introduction

Climate risks that affect human thermal comfort are prevalent in urban environments, as they face the perils of climate extremes. Elevated temperatures have a significant impact on urban metabolism, including building energy consumption, indoor and outdoor thermal comfort, concentrations of harmful pollutants, heat-related mortality and morbidity, sustainability, and survivability levels of low-income households. Additionally, these temperature increases have far-reaching consequences on global economic activity and human well-being (Santamouris, 2020). Many cities have witnessed rapid urbanization and the development of compact building structures, which, coupled with regional climate change, result in excessive summer heating (Khan et al., 2021b). Furthermore, heat waves interact nonlinearly with urban warming, further compromising thermal comfort in cities (Li & Bou-Zeid, 2013) and increasing the extreme precipitation events (Doan et al., 2022).

While urban overheating generally intensifies during heatwaves, some studies suggest reductions; this inconsistency affects heat exchange and urban canyons. Cities of comparable sizes show varied interactions with heatwaves, larger cities like New York City, Washington, DC, and Baltimore experience stronger Urban Heat Island (UHI) amplification during heatwaves, unlike Philadelphia (Ramamurthy & Bou-Zeid, 2017). These findings underscore the inherent link between the pattern of UHI in different cities, its variability, and its interaction with heatwaves, which are influenced by dynamic factors and the background climate (Chew et al., 2021).

Significantly, cities share a majority of the global population and require cooling systems for providing comfortable living conditions during the hottest months (González-Torres et al., 2022). A recent study conducted in 141 cities across China revealed that cities located in warm climatic zones, especially subtropical areas, exhibit a higher intensity of Surface Urban Heat Island (SUHI) during the daytime (Hu et al., 2022). A recent study in India, China, Nigeria that considered both tropical and arid cities concluded that heat island mitigation techniques could delay extreme heat conditions (Huang et al., 2021). However, the study found at night the persistent rise in temperatures can amplify the escalation of health hazards and intensify energy usage, thereby necessitating the implementation of supplementary measures like integrating green/cool roofs with enhanced building insulation to mitigate these concerns.

Unfortunately, urban heating in tropical locations has not received sufficient attention, and studies on this topic remain limited in number, poorly understood, and scientifically unexplored (Chakraborty et al., 2023; Khan & Chatterjee, 2016; Khan et al., 2020, 2022a). Monitoring different

components of surface energy balance (SEB) in many highly urbanized tropical cities remains a significant challenge due to instrumentation limitations, cost, and the need for long-term commitment to measurements. For instance, there are few measurements of solar radiation within net all-wave radiation for daytime urban exchanges of momentum, heat, and water vapor (Ao et al., 2016; Ramamurthy & Bou-Zeid, 2014). Existing studies on tropical urban heating have primarily focused on diurnal and seasonal intensity variations, as well as long-term changes in the urban thermal field resulting from shifts in land use and rapid, unstructured urbanization (Chatterjee et al., 2019).

India has become the most populated country globally (United Nations, 2023). Although research on urban heat mitigation in tropical cities has grown significantly over the last 15 years, studies focusing on urban heat mitigation due to regional climate change are still in their early stages in India's tropical cities. It has been observed that tropical cities have a negative intensity of the UHI during the daytime in dry summer months when compared to their immediate rural surroundings. This contrasts with cities in higher latitudes where such features have not been typically noted (Khan et al., 2021a, 2022a, 2022b).

Beside urban morphology and climate, urban building materials play a fundamental role in the thermal balance of the city. Urban materials with high levels of anthropogenic heat absorb incoming solar radiation and dissipate part of the absorbed heat through convective and radiative processes in the atmosphere, raising the ambient temperatures (Santamouris & Kolokotsa, 2016). Surface characteristics modulate energy partitioning, including net radiation, anthropogenic heat, sensible heat, latent heat, advection, and heat storage. A higher percentage of vegetation promotes latent heat flux at the expense of surface heat storage (Alapaty et al., 1997; Niyogi et al., 1999; Roth, 2007).

Many researchers have proposed various strategies to mitigate urban heat by implementing cool roofs and green roofs in different climate zones, either at the building or city scales (Garshasbi et al., 2023; Khan et al., 2022c; Mohammed et al., 2022; Qi et al., 2020; Santamouris & Vasilakopoulou, 2023; Yang et al., 2018). These technologies reduce the transmission of sensible heat to the air and building envelopes. Most mitigation technologies rely on reflective and chromic materials, greenery, evaporative cooling, solar control systems, and natural heat sinks for heat dissipation (Santamouris et al., 2016). Cool materials, which have a reflectivity up to 80%, are solar reflective materials that maintain lower surface temperatures than common materials with reflectivity up to 65%. Consequently, they effectively mitigate urban heat in warm climates. Several large-scale mitigation projects have shown the potential to reduce peak urban temperatures by up to 3 °C (Santamouris et al., 2016).

Beside this, trees and greenery at the ground level could lower urban overheating. Some studies revealed that urban trees in European cities have lower temperatures compared to the built environment, particularly during summer and hot weather events (Schwaab et al., 2021). Another study reported that on average, the air temperature under trees is 0.8 °C cooler but that tree areas may experience higher temperatures at night. Additionally, the cooling effect varies depending on the species of trees present (Knight et al., 2021).

Moreover, advancements in photonic and plasmonic materials have led to the development of super cool materials with up to 96% solar reflectivity. Their application in the built environment is expected to increase the mitigation potential by up to 5 °C (Santamouris & Feng, 2018) with promising results on low-cost material development (Carlosena et al., 2021). On the other hand, green roofs, also known as rooftop gardens, consist of a vegetation layer grown on a rooftop, providing shade and transpiration cooling, which lowers urban temperatures and reduces heat on the roof surface and in the surrounding air (Shafique et al., 2018). While green roofs are relatively inexpensive to construct, they can incur high maintenance costs over time (Luckett, 2009). The maximum reduction in ambient temperatures achievable with 100% green roofs can be up to 1.4 °C citywide (Li et al., 2014). In the existing scientific literature, the combined strategy of using cool materials and green roofs, referred to as the cool-city model, has also been considered. This integrated approach could potentially reduce ambient temperatures by up to 0.8 °C (Wang et al., 2016).

Cool roofs, green roofs, and the concept of a “cool-city” can contribute to reduce urban heat, enhancing human thermal comfort, and decreasing building cooling loads (Jacobs et al., 2018). Additionally, these cooling strategies can have an impact on the lower atmospheric dynamic (Sharma et al., 2016). This impact manifest as changes in the height of the urban boundary layer due to alterations in heat and moisture exchanges between the urban surface and the lower atmosphere (Miao et al., 2009; Niyogi et al., 2006, 2011; Zhang et al., 2011). Consequently, when assessing the cooling potential, it is crucial to consider the atmospheric boundary layer (Alapaty et al., 2001; Khan et al., 2023b). Changes in local landscape gradients, convection, and dispersion potential, as well as the influence of urban morphologies, energy consumption, and comfort strategies, create a heterogeneous boundary layer structure over and around the city domain (Davies et al., 2007; Han et al., 2015; Masson, 2006; Rigby & Toumi, 2008; Yerramilli et al., 2008). Furthermore, cool roofs and rooftop vegetation influence the vertical mixing by modifying the urban energy balance and lowering boundary layer height during summer peak hours. Thus, considering the

nonlinear interactions between urban heating and regional climate change, which exacerbate heat-related risks in cities, the implementation of urban heat mitigation technologies becomes important (Li & Bou-Zeid, 2013).

According to the latest report of the Intergovernmental Panel on Climate Change (*IPCC AR6 SYR, 2023*), hot extremes, including heatwaves and heavy precipitation events, have increased in East Central Asia and South Asia. The same report indicates that these effects are more significant in equatorial and tropical regions when the projected temperature increase exceeds 3 °C. The various projected global warming levels (GWLs) relative to the period 1850–1900 will result in increased risks of species loss, threats to human health, and a decrease in food production (Fakhruddin et al., 2022). In India, the percentage of species at risk would range between 5 and 10% with a temperature increase of 2 °C. Additionally, with a projected temperature increase of 1.7–2.3 °C, the number of days posing a threat to inhabitants due to high surface temperatures and humidity is at least between 50 and 100 days, which can increase up to 150–200 days in coastal regions.

The temperatures in India have increased substantially in the last century. In the last 150 years, temperature increases of 1 °C in Delhi, 0.7 °C in Mumbai, 1.2 °C in Kolkata, and 0.6 °C in Chennai, have been recorded in some of India’s metropolitan areas. These rising temperatures are further compounded by high humidity (Chatterjee et al., 2019). During Intergovernmental Panel on Climate Change (IPCC, 2018) report on the effects of global warming on cities in 2018, data from two tropical cities, Kolkata and Karachi, were presented. Additionally, both cities experienced their highest heat index in 36 years during the heatwave of 2015 (Matthews et al., 2017). Some Indian cities are already trying to address this issue by implement a Heat Health Prevention Plan (HHPP) or a Heat Action Plans (HAP) which guide citizens and health professionals in the events of extreme heat. The latest HAP for the city Ahmedabad included among its key strategies the promotion of adaptive measures such as launching a city-wide Cool Roof Program (Ahmedabad Municipal Corporation, 2019).

Urban overheating is generally studied through temperature measurements with weather stations, mobile platforms, or on buildings to capture temperature variations across the city (Kaginalkar et al., 2021). Urban weather stations usually provide data on temperature, humidity, wind speed, helping identify urban heat islands. Remote sensing based on infrared sensors measure surface temperature, allows researchers to identify temperature gradients (Aslam et al., 2021; Jain et al., 2016; Zhang et al., 2022). Moreover, building energy consumption monitoring collects data on energy for cooling and heating (Su

et al., 2021). Finally, computational models, such as mesoscale weather models, urban canopy models, and computational fluid dynamics (CFD) models, simulate urban climate and heat transfer processes (Houston & Niyogi, 2007; Mills et al., 2022). These models consider factors like land cover, building materials, urban morphology, and heat exchange to study urban overheating.

The utilization of an integrated Weather Research and Forecasting (WRF)/urban modeling system coupled with Single Layer Urban Canopy Model (SLUCM) for urban thermal mitigation research represents an important aspect of urban climate sustainability. This approach considers multi-scale feedback of urban changes and adequately resolves surface heterogeneity effects in urban canyons (Chen et al., 2011). In the context of assessing urban heat mitigation strategies such as cool roofs, green roofs, and the cool city concept, the WRF model is employed for city-scale analysis, while ENVI-met is utilized for building-scale evaluation (Imran et al., 2018; Li et al., 2014; Wang et al., 2016). Numerical studies have also examined the effectiveness of cool roofs, green roofs, and vegetation in mitigating urban heating in tropical environments (Liu et al., 2017; Mughal et al., 2019; Patel et al., 2021).

2 Materials and methods

This research addresses following questions: (a) What is the cooling potential of green roofs, cool roofs, and cool-city scenarios in the tropical city like Kolkata? (b) Which mitigation technologies effectively balance the thermal environment of tropical cities? (c) What is the comparative cost of the different mitigation measure especially in the tropical urban environments? d) What are the impacts of these mitigation strategies on boundary layer meteorology? Accordingly, this study undertakes numerical experiments for heat mitigation potential using existing material technologies by considering their coupled effect on boundary layer meteorology over Kolkata. The performance of cool roofs, green roofs, and their combined use in the "cool-city" scenario has been assessed through mesoscale WRF-urban modeling. The cooling capacity and thermal performance of different scenarios are presented based on a high-resolution city-scale WRF/SLUCM simulation. Furthermore, the research examines each heat mitigation scenario's ability to reduce urban heat and enhance the city's cooling potential at a city scale. In particular, the performance of eight different heat mitigation scenarios for improving urban thermal balance by increasing the albedo or the rooftop green fraction, as well as a combination of best practices known as "cool-city" (reflective surface and rooftop green fraction), is studied. For a tropical city like Kolkata, it is unrealistic to compare cool surfaces and green surfaces outside of the roof area as the lack of open spaces in urban morphologies in high-density urban

areas of Kolkata does not support green surfaces besides their use as a rooftop. As a result, we only considered the green fraction of the rooftop.

2.1 WRF model configuration

In April, India experiences summer premonsoon conditions, resulting in significantly high temperatures across most parts of the country (Niyogi et al., 2018). In Kolkata, the recorded minimum temperature was approximately 25.1 °C, while the maximum temperature reached 39.2 °C. Throughout the simulation period, the average humidity remained above 50%. There were no significant opportunities for the humidity to increase, leading to an unusually dry and hot climate that was expected to persist throughout the simulation. The soil moisture level varied from moderately wet to moderately dry. The average surface wind speed was measured at 3.6 km/h, predominantly coming from the south-southeasterly direction. Moreover, in residential buildings, there is water storage available on the roofs, and this is typically seen in most buildings across the city.

We used the WRF/SLUCM mesoscale urban climate model with one-way nesting for a parent domain and two nested domains centered over Kolkata (22.57°N, 88.36°E) with grid resolutions of 18 km, 6 km, and 2 km (Fig. 1) at the city scale (Khan et al., 2022a, 2022b). The city of Kolkata has been centered over the innermost domain to capture the heat mitigation cooling potential at the city scale, with a grid resolution of 2 km. The spatial resolution was chosen primarily based on computational resources and access to the land use dataset for developing and interpreting the results. Table 1 summarizes the model physics parameterizations used in this study. Remotely sensed Landsat data with a spatial resolution of 30×30 m are used to recreate the simulation's new and updated land use (LU) scheme. However, it has to be noted that the process of extracting built-up areas using Landsat data is difficult in developing countries, especially in tropical regions (Khan et al., 2019). The updated LU map was developed with R-programming and ArcGIS 10.1 using the machine learning support vector machine (SVM) technique (Khan et al., 2022a, 2022b) and overlaid on the default Moderate Resolution Imaging Spectroradiometer (MODIS) LU (Fig. 2). As a result, the new LU map on the default MODIS LU can precisely capture the precise urban processes to portray the actual scenarios of building settings in the city of Kolkata.

The initial and boundary conditions were based on the available high-resolution dataset from the National Centers for Environmental Prediction's (NCEP) operational Global forecasting system (GFS) (NCEP Central Operations, n.d.), whose analysis and forecast grids are on a 0.25°×0.25° grid resolution to force the WRF/SLUCM (Khan et al., 2022a, 2022b). The grids were divided into two analysis and forecast time steps (a) at 3

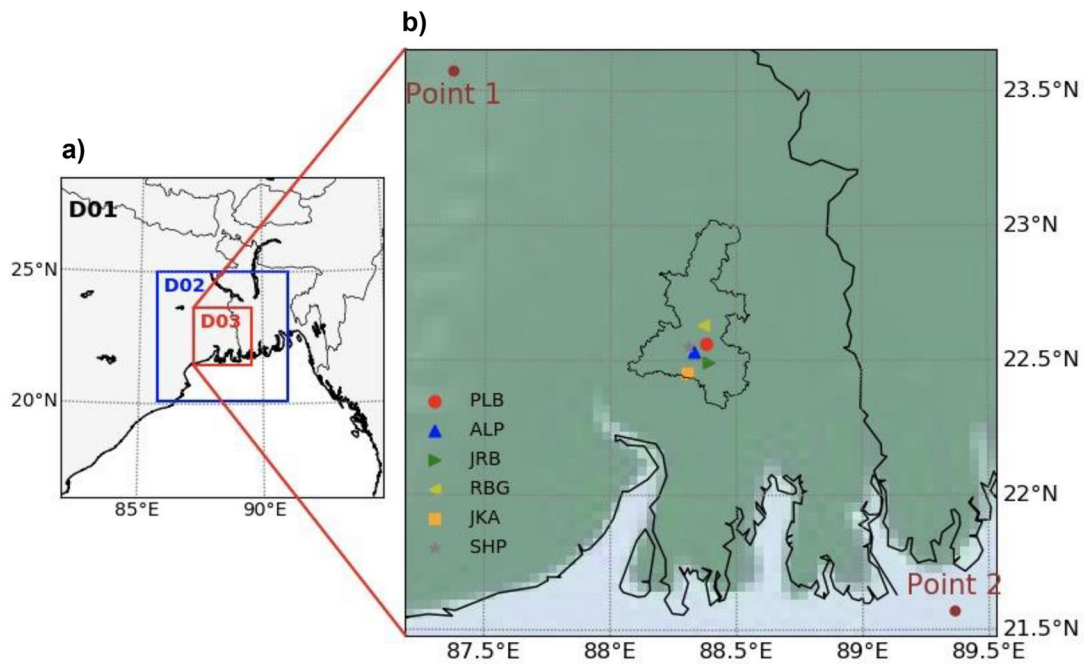


Fig. 1 WRF domain configuration **a** shows dynamical downscaling with D01 as the outermost parent domain with 18 km grid resolution, D02 with 6 km resolution, and innermost D03 with 2 km grid resolution; **b** innermost D03 with 2 km resolution which includes the Kolkata metropolitan area (KMA). For present simulations, only updated LULC (31) corresponding to high-intensity residential was used for mitigation purposes. The point 1 (23°57'; 87°36') and 2 (21°57'; 89°36') are the points used for drawing cross-section lines between them to analyze the changes in meteorological conditions towards the vertical direction. Besides, six local meteorological observations were located by station codes for Palmer Bridge (PLB), Alipore (ALP), Jora Bridge (JRB), Ratanbabu Ghat (RBG), Joka (JKA), and Shibpur (SHP) and corresponding urban morphology in the lower panel

Table 1 WRF/SLUCM Model configuration

| Configuration | Domain 01 (D01) | Domain 02 (D02) | Domain 03 (D03) |
|---------------------------------|---|-----------------|-----------------|
| Version | ARW-WRF V 4.0 | | |
| Initial and boundary conditions | NCEP GFS 0.25° × 0.25° | | |
| Run time | 6 April 00:00 h, 2020 to 8 April 00:00 h, 2020 IST | | |
| Period for analysis | 7 April 00:00 h, 2020 to 8 April 00:00 h, 2020 IST | | |
| Grid distance (km) | 18 | 6 | 2 |
| Time step (sec) | 108 | 36 | 12 |
| Grid number | 75 × 75 | 91 × 91 | 121 × 121 |
| Number of vertical layers | 40 layers | | |
| Microphysics | Purdue-Lin scheme (Lin et al., 1983) | | |
| Surface layer model | Noah-LSM+ Single layer UCM (Chen & Dudhia, 2001; Kusaka et al., 2001) | | |
| Turbulence | TKE scheme (Mellor & Yamada, 1974) | | |
| Short-wave radiation | Dudhia scheme (Dudhia, 1989) | | |
| Long-wave radiation | RRTM scheme (Mlawer et al., 1997) | | |
| Planetary boundary layer | Asymmetrical Convective Model version 2 (ACM2) (Pleim, 2007) | | |
| Cumulus parameterization | Kain-Fritsch (KF) scheme (Kain, 2004; Zheng et al., 2016) | | |

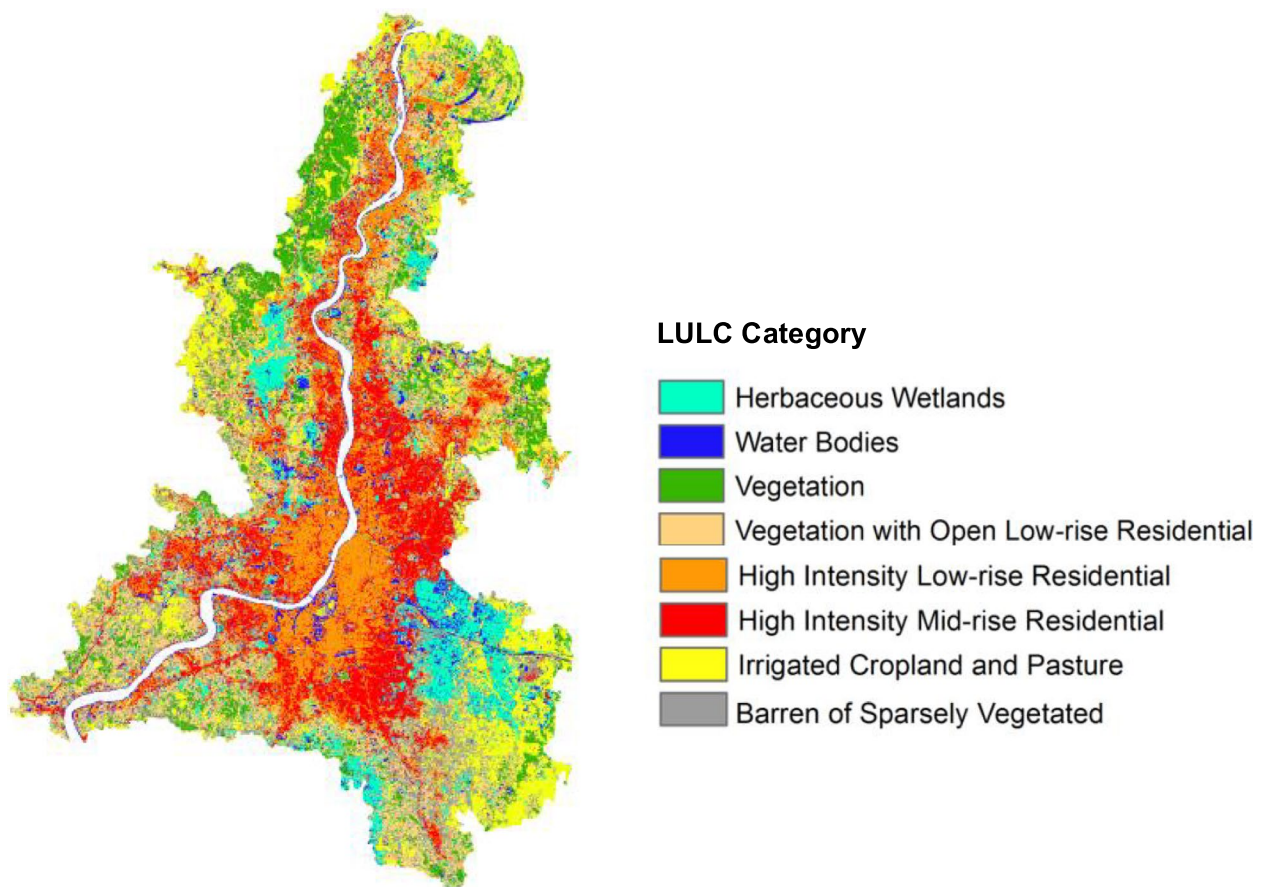


Fig. 2 The WRF model domain with default MODIS land use categories. (Khan et al., 2021b)

hourly temporal intervals ranging from 0 to 240 and (b) at 12 hourly temporal intervals ranging from 240 to 384. The model forecast ran daily at 00:00, 06:00, 12:00, and

18:00 Universal Time Coordinated (UTC). The simulations were for cloud-free skies and a relatively calm wind setting, corresponding to two summer days in Kolkata.

These conditions represent the typical settings for urban heating with limited ventilation potential. We used a 48-h simulation run from April 6 to April 8, 2020, to assess the urban cooling potential. The output of standard meteorological parameters for the innermost urban domain was used to perform a post-processing evaluation of various heat mitigation measures. From the 48-h simulation, the first 24 h were considered the model stability spin-up time and, as a result, were excluded from the post-processing analysis (Alapaty et al., 2001; Niyogi et al., 2006).

The radiative trapping and energy conservation equations for the roof, wall, and ground were solved in the WRF/SLUCM. Each urban facet had its own thermal and radiation parameters, such as albedo, emissivity, conductivity, and heat capacity. The surface temperature of each facet (roof, wall, and ground) in the WRF/SLUCM was derived from surface energy balance (Kusaka et al., 2001), as shown in Eq. (1).

$$R_n = H + E + G \tag{1}$$

where is the R_n surface net radiative flux density, H is the sensible heat flux, E is the sensible heat flux, and G is the heat flux into the ground.

At the bottom layer, the boundary condition is either zero heat flux or constant temperature. The ground heat flux $G_{z,i}$ and interior temperature $T_{z,i}$ at depth z to i the surface can be calculated using (Kusaka et al., 2001) Eqs. (2) and (3):

$$G_{z,i} = \lambda_i = \frac{\partial T_{z,i}}{\partial z} \tag{2}$$

$$\frac{\partial T_{z,i}}{\partial t} = -\frac{1}{\rho_i c_i} \frac{\partial G_{z,i}}{\partial z} \tag{3}$$

where λ_i is the interior thermal conductivity and $\rho_i c_i$ is the volumetric heat capacity of the surface i . The subscript denotes the roof, wall, or ground (road).

The averaged roof temperature T_{roof} was calculated (Sharma et al., 2016) as in Eq. (2) for cool roof and green roof, respectively (Fig. 3):

$$T_{roof} = (F_{coolroof})T_{coolroof} + (1 - F_{coolroof})T_{conventionalroof} \tag{4}$$

$$T_{roof} = (F_{greenroof})T_{greenroof} + (1 - F_{greenroof})T_{conventionalroof} \tag{5}$$

where $F_{cool/greenroof}$ is the green/cool roof fraction, $T_{cool/greenroof}$ represents the cool/green roof temperature, and $T_{conventionalroof}$ is the conventional roof temperature. Canyon temperature T_{canyon} (2 m) was calculated as follows using Monin–Obukhov (M–O) similarity theory in Eq. (3):

$$T_{canyon} = T_{surface} + (T_{Model} - T_{surface}) \frac{U}{U^*} \tag{6}$$

where $T_{surface}$ denotes the surface temperature, T_{model} represent the first layer model level, U is the velocity at the first model level and U^* is the friction velocity at 2 m.

The surface energy balance in Eq. (7) gave the total net radiation on the roof surface for any heat mitigation measure:

$$R_n = SW_{in}(1 - \alpha) + LW_{in} + LW_{Out} \tag{7}$$

where SW_{in} denotes incoming shortwave radiation, α represents albedo, and LW_{in} is the longwave incoming and outgoing radiations.

Furthermore, the dynamically coupled green roof algorithm with four different layer structures calculated the green roof’s temperature. WRF/SLUCM was used in conjunction with the green roof algorithm. From 18:00 to 20:00 local time (LT), the WRF green roof model also used an irrigation algorithm to improve soil moisture over the urban surface and green roofs (Yang et al., 2015). The green roof is covered by grass, assuming leaf area index (LAI)=2, albedo of green roof (α_{gr})=0.154, minimal stomatal resistance of the vegetation ($R_{s,min}$)=40,

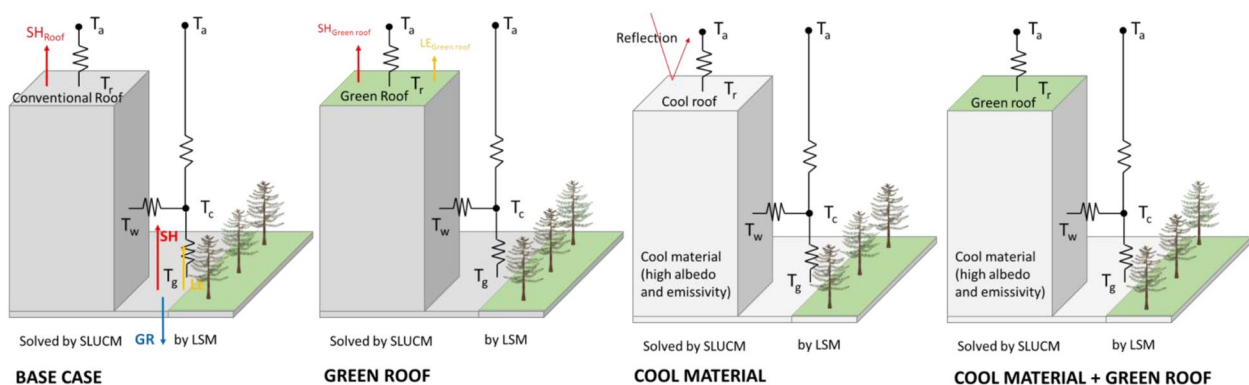


Fig. 3 Schematic diagram representing the WRF urban grid cell with SLUCM and Land Surface Model (LSM) and their interaction with temperatures and surface energy components of roof, wall, ground (road) in urban cooling simulations for base case, green roof, cool roof (cool materials) and cool-city (cool materials and green roof)

Table 2 Numerical design for the base case and mitigation studies

| Numerical design | Type of roof | Mitigation strategies (high-density residential areas) | | |
|----------------------|---------------------|--|--|--------------------------|
| | | Albedo fraction | Emissivity fraction | Green fraction (rooftop) |
| Base case | Conventional | Roof 0.20 Wall 0.20 Ground (road) 0.20 | Roof 0.90 Wall 0.90 Ground (road) 0.95 | - |
| Cool roof-A | Cool roof | Roof 0.65 Wall 0.20 Ground (road) 0.20 | Roof 0.90 Wall 0.90 Ground (road) 0.95 | - |
| Cool roof-B | Cool roof | Roof 0.85 Wall 0.20 Ground (road) 0.20 | Roof 0.90 Wall 0.90 Ground (road) 0.95 | - |
| Cool roof-C | Cool roof | Roof 0.55 Wall 0.20 Ground (road) 0.20 | Roof 0.90 Wall 0.90 Ground (road) 0.95 | - |
| Green roof-A | Green roof | Roof 0.65 Wall 0.20 Ground (road) 0.20 | Roof 0.90 Wall 0.90 Ground (road) 0.95 | 0.25 |
| Green roof-B | Green roof | Roof 0.65 Wall 0.20 Ground (road) 0.20 | Roof 0.90 Wall 0.90 Ground (road) 0.95 | 0.50 |
| Green roof-C | Green roof | Roof 0.65 Wall 0.20 Ground (road) 0.20 | Roof 0.90 Wall 0.90 Ground (road) 0.95 | 0.75 |
| Green roof-D | Green roof | Roof 0.65 Wall 0.20 Ground (road) 0.20 | Roof 0.90 Wall 0.90 Ground (road) 0.95 | 1.00 |
| Cool city (combined) | Cool and green roof | Roof 0.85 Wall 0.20 Ground (road) 0.20 | Roof 0.90 Wall 0.90 Ground (road) 0.95 | 1.00 |

and initial green roof soil moisture (SM)=0.2 m³ m⁻³ (Zonato et al., 2021). However, green roof also expects to irrigate the roof surface vegetation in the period 01:00–03:00 LT. A total of 25L m⁻² of water is set at the surface of the uppermost green roof layer per week (de Munck et al., 2018; Khan et al., 2023a).

2.2 Numerical design for heat mitigation

Cool roofs, green roofs, and cool-city (combined strategy) have proven promising options for reducing extreme urban heat. Reflective and transpiration cooling measures have profoundly impacted incoming solar radiation, altering urban energy balance. As a result, this modifies the heat flux partition, Bowen ratio, and evaporative fraction over the urban domain. It has been observed that changes in urban energy balance can impact available soil moisture exchange between the canopy layer and the lower atmosphere, which in turn impacts conduction, convection, and advection at the city scale (Niyogi et al., 2020).

Due to the peculiarities of urban energy balance in tropical urban environments, there is still a lack of proper knowledge to deploy the most appropriate heat mitigation technologies suitable for improving

Table 3 Prices found in the market for cool roofs and green roofs. An estimation is made for the cool-city scenario

| Solution | Price range (\$/m ²) |
|----------------|----------------------------------|
| Cool roofs | |
| Basic | 37.7–53.8 |
| Standard | 53.8–145.3 |
| Best quality | 183–290 |
| Green roofs | |
| Intensive | 226–409 |
| Semi-intensive | 161.5–322.9 |
| Extensive | 107.6–215.3 |
| Cool city | |
| Cool-city | 129.2–236.8 |

the thermal environment of tropical coastal cities. To numerically assess the urban cooling potential of different types of cool roofs, green roofs, and cool-city, each urban grid cell is replaced with assumed scenarios value with a realistic fraction of the surfaces that can be cool/green listed in Table 2: one conventional roof (control scenario), and eight mitigation scenarios that include

three cool roofs with different reflectivity values (A, B, and C), four green roofs with different rooftop green fraction (A, B, C, and D) and an optimal combination of the considered scenarios (cool-city). Furthermore, the albedo or green roof fraction is a single fraction that was uniformly applied to all urban grid cells (Feng et al., 2022).

While considering the cooling potential, it is also important to take economic factors into account when evaluating heat mitigation solutions, particularly in retrofit scenarios (Bixler et al., 2022). The prices of various mitigation scenarios vary depending on the solution. Cool roofs can be implemented through the application of cool material paints, membranes, concrete, or clay tiles with cool materials. By referring to the information available in the Cool Roof Rating Council directory (CRRC Roof Directory, n.d.), we identified a range of solutions with different solar reflectance and thermal emittance that align with the selected scenarios as in Table 2. Similarly, the effectiveness of green roof solutions is dependent on the specific type of green roof chosen, whether it is intensive, semi-intensive, or extensive. Table 3 provides an overview of the average prices observed in the USA market for the different solutions, these prices might be lower in India.

2.2.1 Conventional roof (control case)

For the conventional low-slope roof, the insulation is considered beneath the roof membrane. As a result, the large spectrum of incoming solar energy (net radiation) is translated into sensible heat flux, which raises the surface temperature of a conventional roof and thus heats the building environment. In this study, the value of albedo in the conventional roof (control scenario) is assumed to be 0.2, and the default urban morphology parameters (street width, aspect ratio, and building heights, among others) associated with the urban category are assumed to be representative on average (Bogoslovskij, 1982; Feng et al., 2022).

2.2.2 Cool roof

The technology-based cool or reflective roofs have primarily been white and have a higher reflective value than conventional roofs. In the present study, however, we used cool roofs and first- and second-generation roof

materials for city-scale simulations. The first generation of cool roofs is typically made from available natural materials such as chromium oxide pigments or white aggregates that are appropriate for use in asphalt concrete pavement such as silica gravel, quartz, white stone, white marble, and some granite. These first-generation cool roof materials had a reflectivity of up to 0.75, which is a significant reduction of the solar absorption of the building roofs (Bretz et al., 1992; Doulos et al., 2004; Reagan & Acklam, 1979). Second-generation cool roof materials, on the other hand, were developed based on artificial white materials with higher reflectivity values close to 0.85, and these technologies established a heat-shedding effect in the building environment (Kolokotsa et al., 2012; Santamouris et al., 2008; Mohammed et al., 2021; Synnefa et al., 2011). In addition, by shimmering shortwave radiation from high albedo surfaces, a cool roof can reduce a significant portion of the available net inflow radiation on the rooftops of urban buildings. Both generations of cool roofs were evaluated in three test cases involving cool roof strategies.

2.2.3 Green roof

The green roofs used in buildings are entirely or partially covered by vegetation on the top of the growth substrate. These green roofs have been classified into three basic types: (a) intensive green roofs, (b) semi-intensive green roofs, and (c) extensive green roofs (Akbari & Kolokotsa, 2016; Vijayaraghavan, 2016). Green roofs in the WRF-urban modeling system have a four-layer structure with a total depth of 0.5 m: (a) topsoil layer (0.05 m), (b) soil layer (0.10 m), (c) growing medium layer (0.15 m), and (d) concrete roof (0.20 m) in the urban parameters table. For green roof simulations with semi-intensive roofs, we replaced the roof surface with an assumed rooftop green fraction of 0.25, 0.50, 0.75, and 1.00 for each roof (green roof-A, green roof-B, green roof-C, and green roof-D), and repeated these simulations to evaluate cooling using sensitive tests.

2.2.4 Cool city (combined scenarios)

It has been well established that increasing the urban albedo and vegetation fraction on roofs results in cooling effects (Khan et al., 2022a). However, these measures also

Table 4 Characteristic of observed stations

| Stations | Code | Latitude | Longitude | Surrounding environment |
|----------------|------|------------|------------|--|
| Alipore | ALP | 22°32'09"N | 88°19'51"E | Mixed vegetation with settlements |
| Ratanbabu Ghat | RBG | 22°37'50"N | 88°21'58"E | Dense settlements near the river |
| Shibpur | SHP | 22°33'23"N | 88°18'07"E | Mixed vegetation with settlements |
| Palmer Bridge | PLB | 22°33'48"N | 88°22'41"E | Liner settlements along roads networks |
| Jora Bridge | JRB | 22°29'40"N | 88°23'26"E | Dense settlements |
| Joka | JKA | 22°27'19"N | 88°17'30"E | Dense settlement |

have a feedback on the urban environment. High albedo can reduce moisture availability in the lower atmosphere, whereas higher vegetation fraction on the roof can lead to low-level urban pollution. As a result, this study used a combined strategy for lowering negative impacts on urban climate at the city scale as a compensatory strategy. The cool-city, as a combined scenario, took the best-performing strategies (Cool roof-B and Green Roof-D) into account. The urban cooling potential of cool roofs and green roofs for improving the urban thermal environment has been investigated, and it is entirely dependent on city size, geographic location, urban land use, building materials, and building morphologies. However, when greenery and reflective materials are combined, they can yield more significant cooling potential and environmental benefits. This can also be a co-benefit for energy demands and urban sustainability at the building and city scales (Dai et al., 2023; Santamouris et al., 2016).

2.3 Base model evaluation

We compared the 2-m air temperature of the base case simulation from the innermost domain with selected

local meteorological observations over the urban domain for validation and evaluation of base model performance during the simulation period. We used the observations from six meteorological stations (Fig. 1) maintained by the Kolkata Municipal Corporation (KMC) across different urban land use categories (Table 4). In addition, the Weather Kolkata (<http://weatherkolkata.in/>) hourly climatological dataset provides in situ meteorological observations (Feng et al., 2021; Khan et al., 2022a, 2022b).

The Taylor Diagram was used to assess how three complementary model performance statistics, namely the correlation coefficient (R), standard deviation (SD), and root-mean-square error (RMSE). The results vary concurrently for the six local meteorological stations compared to model results (Fig. 4). These three statistics were plotted in two dimensional to form a relationship using the law of cosines. The best complementary agreement of 2-m air temperature over the urban grid was found in base model results and local observations for Alipore (ALP) and Shibpur (SHP).

In addition, the statistics mean bias error (MBE), mean absolute error (MAE), root mean square error (RMSE),

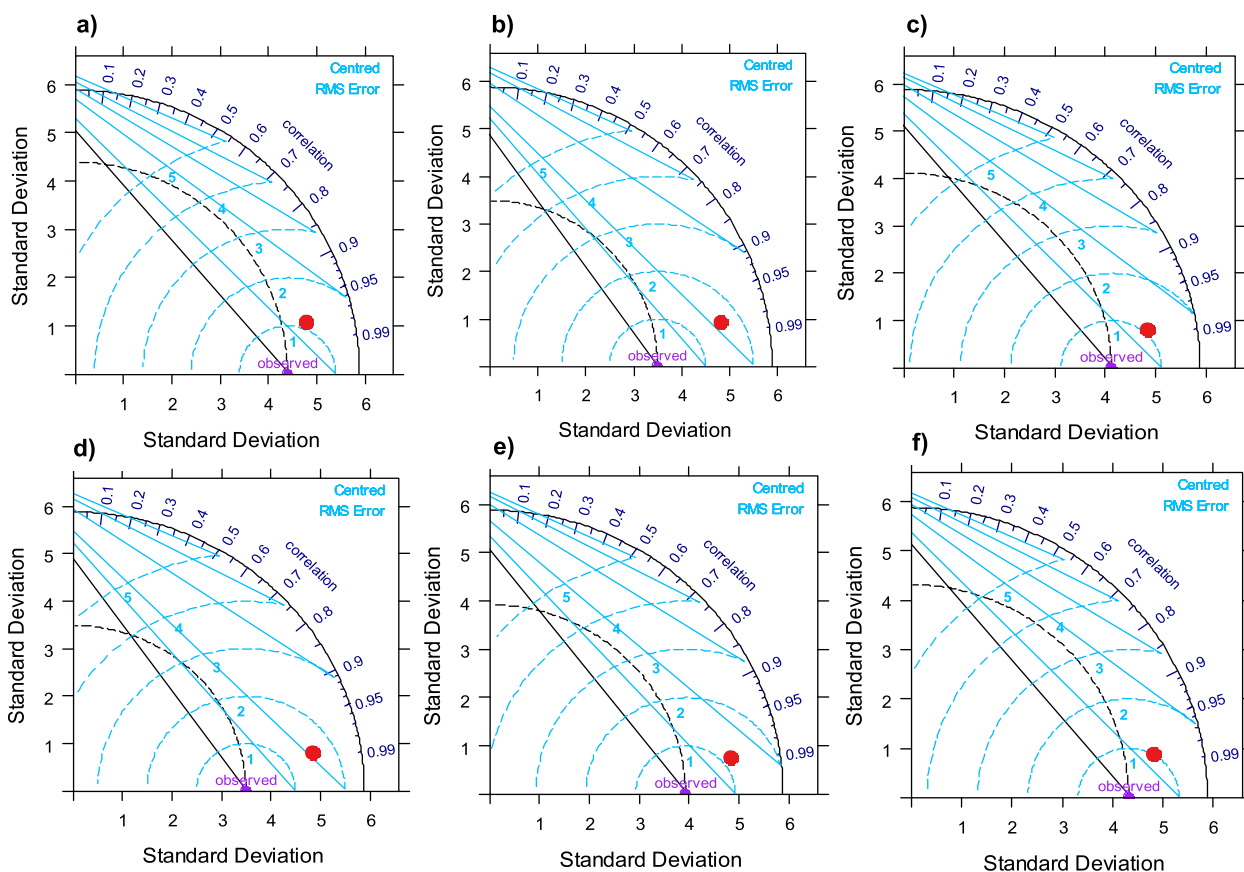


Fig. 4 A statistical summary of agreement and validation patterns between local meteorological observations **a** Alipore, **b** Ratanbabu Ghat, **c** Shibpur, **d** Palmer Bridge, **e** Jora Bridge, and **f** Joka and model simulations in terms of their correlation, root-mean-square difference, and the ratio of their variances

Table 5 Base model evaluation / comparison of the simulation results with observation data

| Parameters | ALP | RBG | SHP | PLB | JRB | JKA | Average |
|-------------------------|------|------|------|------|------|------|---------|
| Correlation coefficient | 0.97 | 0.98 | 0.98 | 0.98 | 0.99 | 0.99 | 0.98 |
| Mean bias error | 0.4 | 1.0 | 0.5 | 0.6 | 0.8 | 1.0 | 0.72 |
| Mean absolute error | 0.43 | 1.0 | 0.46 | 0.61 | 0.80 | 1.01 | 0.72 |
| Root mean square error | 1.2 | 1.9 | 1.2 | 1.7 | 1.4 | 1.4 | 1.5 |
| Index of agreement | 0.98 | 0.95 | 0.98 | 0.96 | 0.97 | 0.97 | 0.96 |

and correlation coefficient (R) for hourly 2-m air temperature between the base model and WRF/SLUCM over the urban grid were summarized and compared in Table 5. The temperature observed at different stations was generally accurately captured by the coupled WRF/SLUCM model ($r=0.98$). The results of the base case simulation were statistically significant ($p < 0.05$) and replicated well the urban standard meteorological fields for the six local meteorological observations. The results of MBE and RMSE values for 2-m air temperature ranged from 4 °C to 1 °C and 1.2 °C to 1.9 °C, respectively. These statistical summaries showed that the local observations from Alipore (ALP) and Shibpur (SHP) highly correlated with the base model results for 2-m air temperature over the urban domain. This result was consistent with previous results obtained from the Taylor Diagram. The 2-m air temperature over the urban domain was slightly overestimated by the WRF/SLUCM. This was primarily due to an error in accurately capturing solar radiation over the urban domain. Model biases are most likely caused by two critical factors: (a) a lack of static urban data, proper meteorological inputs, and their spatial and temporal resolution (Patel et al., 2023), and (b) variability in model parametrization, calibration, and stability. However, the validation of the base model with local observations via statistical analysis confirmed that the base model was sufficient to capture the urban meteorological fields and can be helpful in subsequent heat mitigation modeling and analysis.

The maximum/minimum temperatures in the simulated base case for the 2-m ambient environment, air, surface, roof, and canopy were 39.2/25.1 °C, 38.3/25.2 °C, 42.6/25.2 °C, 54.5/24.1 °C, and 47.6/26 °C, respectively. Furthermore, the main climatic parameters for the diurnal scale were temperatures (ambient environment, surface, roof, and canopy) and heat fluxes (latent heat, sensible heat, and heat storage).

The intensity of the UHI over the urban domain in Kolkata was captured by the model on a diurnal scale. The UHI intensity was calculated by comparing a fixed urban surface to nearby various local surfaces and then averaging the value of differences to obtain the actual average intensity. The average UHI intensity showed a distinct diurnal variation with higher fluctuations. Positive UHI intensity was found at night (2.1 °C), and negative UHI intensity was found during the day (1.8 °C) over the urban domain (Fig. 5). This was primarily because the majority of Kolkata’s urban materials are conventional types with superior heat retention capacity during the day and higher release capacity during the night. This is due to two reasons. The first is related to the heat capacity of commonly used city building materials, which absorb heat during the day and release it at night, and the second is related to the sky view factor, which acts as a barrier to the emission of long-wave radiation to upper air during the night. In order to reduce the amount of heat emitted as long-wave radiation at night (Nichol, 1996). Other

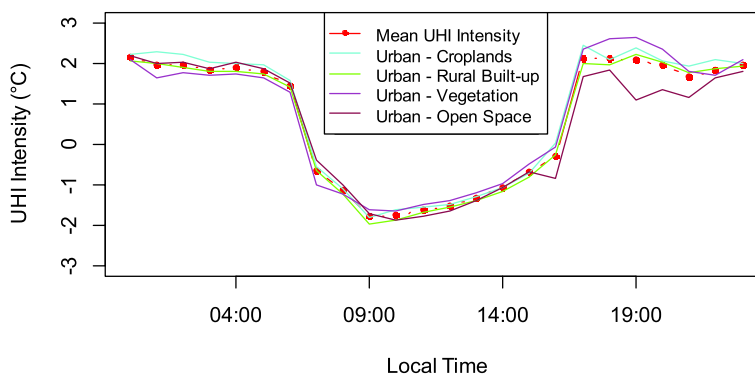


Fig. 5 Urban heat island intensity (UHII) for diurnal scale using fixed urban point to variable rural landscapes (model evaluation)

factors like climate and geographic location cannot be overlooked. Furthermore, because heat is released more slowly in urban areas than in rural areas, building masses create a positive and warm surface island at night.

3 Results

We extracted the grid values from the simulation results' innermost domain to assess the urban cooling potential. For the analysis, the mean values of each parameter were used. Roof, wall, and ground (road) surface modifications altered the radiation balance of the buildings, moisture exchange, and the city's local surface energy balance. The results of city-scale simulations for the peak hour (14:00LT) of a typical hot and clear sky day (7 April 2020) during the pre-monsoon season were presented and discussed for cool roofs (A, B, and C), green roofs (A, B, C, and D), and cool city.

To evaluate the different mitigation scenarios, we calculated and compared them with the base case. The following heat fluxes and temperatures were calculated: sensible heat, latent heat, heat storage, 2-m ambient temperature, surface temperature, air temperature, roof

temperature, and urban canopy temperature. Besides the maximum and minimum temperature decrease, the temperature gradient and the dimensionless temperature gradient are also presented. Finally, the urban cooling effects on the boundary layer structure are presented for the different scenarios.

3.1 Urban heat mitigation technologies and urban energy balance

Changes in the albedo, emissivity, and green fraction in urban grid cells affects the surface energy components, advection, and the urban surface's heat storage capacity. In this study, standard approaches for mitigating urban heating include using reflective materials or rooftop greenery. The material technology reduces the amount of solar radiation absorbed by urban facets, while the latter modifies the surface energy flux partitioning (Bowen ratio). The WRF/SLUCM solves the radiative trapping and energy conservation equations for each urban surface (roof, wall, and road); each facet has its own thermal and radiation parameters (albedo, emissivity, conductivity, and heat capacity) over the city domain (Kusaka et al., 2001). The changes in

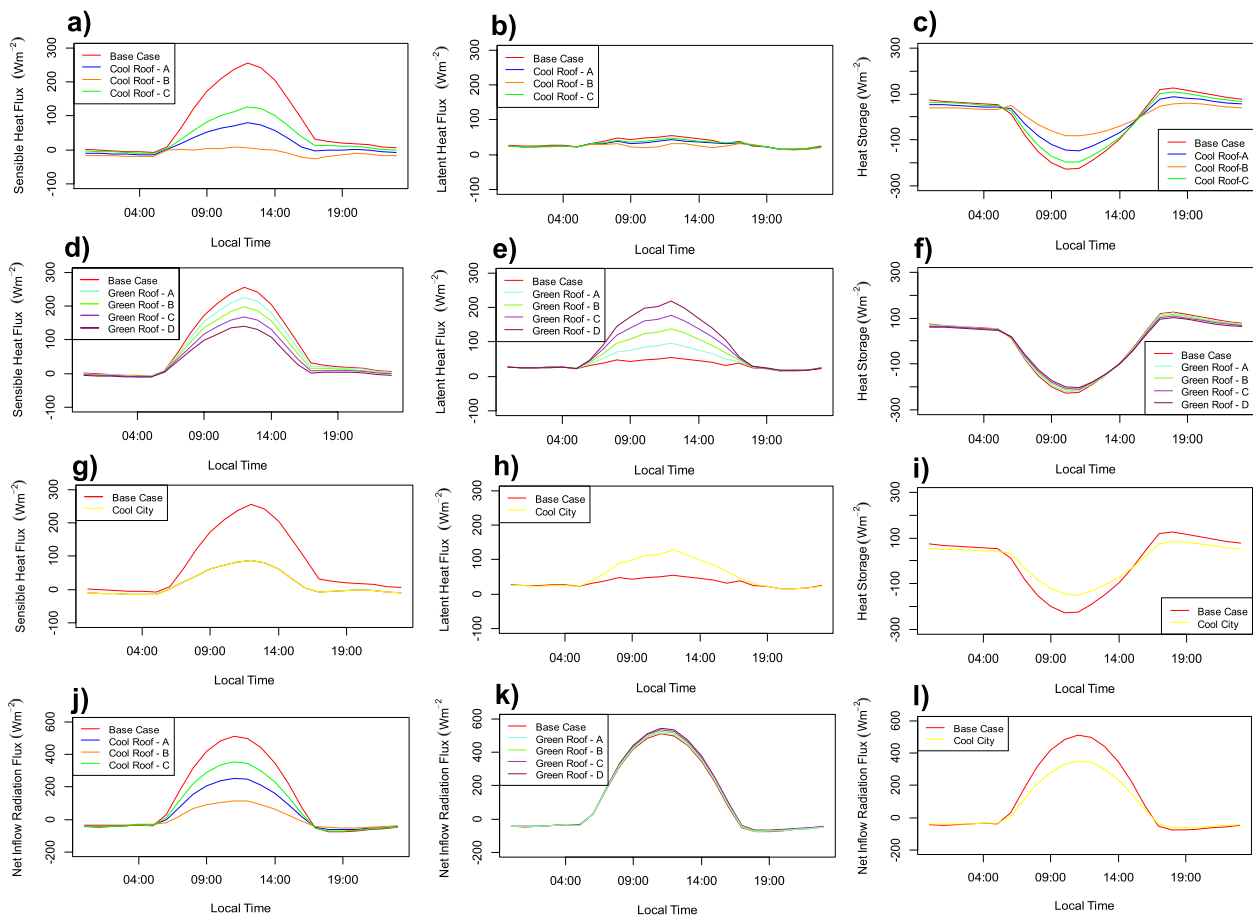


Fig. 6 Comparison of simulated heat fluxes for different scenarios at a diurnal scale (sensible heat flux, latent heat flux, and heat storage): **a-c** cool roofs, **d-f** green roofs, and **g-i** cool-city. Figures **(j-l)** show the net inflow radiation flux for cool roofs, green roofs, and cool-city

energy flux components over high-intensity residential building environments in different sensitivity experiments compared to the base model are shown in Fig. 6. When reflective materials are used instead of rooftop vegetation, the results show that each energy partition component is considerably altered. The urban energy balance in the near-surface urban environment can be used to determine the effect of UHI in an urban area. This can be calculated using Eq. (5) of surface energy balance (Oke, 1988).

$$Q^* + Q_F = Q_L + Q_H + \Delta Q_S + \Delta Q_A \tag{8}$$

where Q^* is the net-all-wave radiation; Q_F is the anthropogenic heat release; Q_L is the latent heat flux; Q_H is the sensible heat flux; ΔQ_S is the heat storage; ΔQ_A is the advection. This study considered and discussed only sensible heat, latent heat, and heat storage.

3.1.1 Sensible heat change

The highest reductions in sensible heat occurred during peak hours, and the values (Table 6) are: -175.5 Wm^{-2} , -250.5 Wm^{-2} , -128.1 Wm^{-2} , -29.3 Wm^{-2} , -58.1 Wm^{-2} , -86.8 Wm^{-2} , -115.2 Wm^{-2} , and -169 Wm^{-2} for cool roof-A, cool roof-B, cool roof-C, green roof-A, green roof-B, green roof-C, green roof-D, and cool-city, respectively. The cool roof-B and cool-city yielded the highest potential for sensible heat reduction over the urban environment as -250.5 Wm^{-2} and -168.9 Wm^{-2} , respectively. Nevertheless, when a green roof is combined with cool materials, the sensible heat reduction increases from 225.8 Wm^{-2} to 86.8 Wm^{-2} and latent heat flux from 55.2 Wm^{-2} to 128 Wm^{-2} due to coupling effects reflections and evapotranspiration. Green roof-D is a promising approach to reduce sensible heat during peak hours up to 255.7 Wm^{-2} to 140.6 Wm^{-2} and increased latent heat flux up to 55.2 Wm^{-2} to 218.8 Wm^{-2} (Fig. 6). The

Table 6 Maximum heat flux reduction (scenario minus base case) for the different heat mitigation technologies. H is the sensible heat flux, E is the latent heat flux, and G is the heat flux into the ground, and R_n is the net radiative flux density to the surface

| Scenarios | $H (\text{Wm}^{-2})$ | $E (\text{Wm}^{-2})$ | $G (\text{Wm}^{-2})$ | $R_n (\text{Wm}^{-2})$ |
|--------------|----------------------|----------------------|----------------------|------------------------|
| Cool roof-A | -175.8 | -13.6 | -41.3 | -256.2 |
| Cool roof-B | -250.5 | -28.7 | -73.1 | -399.9 |
| Cool roof-C | -128.1 | -8.1 | -18.4 | -156.8 |
| Green roof-A | -29.3 | -0.3 | -6.4 | -0.07 |
| Green roof-B | -58.1 | -0.6 | -12.9 | -0.09 |
| Green roof-C | -86.8 | -0.9 | -19.4 | -0.10 |
| Green roof-D | -115.2 | -1.7 | -26.0 | -0.66 |
| Cool city | -169.0 | -3.4 | -44.9 | -162.3 |

difference between the base model and green roof-D for sensible heat reduction is -115.1 Wm^{-2} (Table 6). However, green roofs did not significantly reduce the ambient temperature over the urban domain by adding additional moisture from evapotranspiration and irrigation as compared to cool roofs-B and cool city. Results also show that green roofs redistribute heat over the urban domain. However, cool roofs function as cut-off input radiation, reducing the input energy. For example, cool roof B can reduce a negative sensible heat flux from 10 Wm^{-2} to 20 Wm^{-2} at peak hours.

3.1.2 Latent heat change

The reduced latent heat is at peak hour, and the values were -13.6 Wm^{-2} , -28.7 Wm^{-2} , -8.1 Wm^{-2} , -0.3 Wm^{-2} , -0.6 Wm^{-2} , $0-0.9 \text{ Wm}^{-2}$, -1.7 Wm^{-2} , and -3.4 Wm^{-2} for cool roof-A, cool roof-B, cool roof-C, green roof-A, green roof-B, green roof-C, green roof-D, and cool city (Table 6), respectively. Cool roofs reduce urban heating primarily by reducing the solar radiation absorbed by urban surfaces, so net radiation decreases during the day, with the maximum decrease occurring during peak hours. On the other hand, green roofs mainly reduce sensible heat by increasing latent heat through evapotranspiration. However, results show that latent heat did not increase significantly even using the irrigation on green roof algorithm, due to the low evapotranspiration values.

3.1.3 Heat storage change

Consistent with the results for the heat fluxes, the maximum reduction in heat storage is also concurrent to the peak radiation levels, and the values were -41.3 Wm^{-2} , -73.1 Wm^{-2} , -18.4 Wm^{-2} , -6.4 Wm^{-2} , -12.9 Wm^{-2} , -19.4 Wm^{-2} , -26 Wm^{-2} , and -44.9 Wm^{-2} for cool roof-A, cool roof-B, cool roof-C, green roof-A, green roof-B, green roof-C, green roof-D, and cool city, respectively. Moreover, the maximum decrease of net radiation occurred at peak hour, and the values were -256.2 Wm^{-2} , -399.9 Wm^{-2} , -156.8 Wm^{-2} , and -162.2 Wm^{-2} for cool roof-A, cool roof-B, cool roof-C, and cool city. In other words, the net radiation did not change, and the energy was redistributed. The impact of rooftop vegetation on net radiation is low compared to cooling materials effects.

3.2 Urban heat mitigation and their temperature reduction potential

As previously mentioned, reflective materials with white coatings, rooftop vegetation, and their combination have been used and advocated as cost-effective measures to reduce urban heat and building cooling loads in

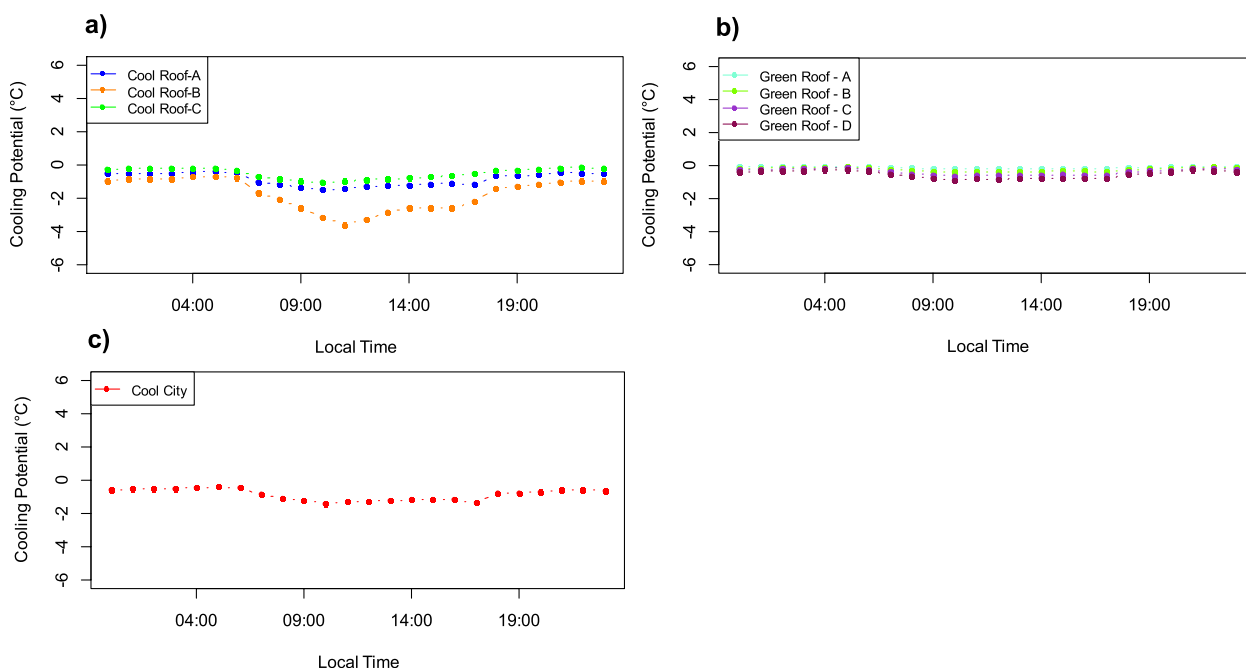


Fig. 7 Cooling potential of different heat mitigation strategies at a diurnal scale for **a** cool roofs, **b** green roofs, and **c** cool city

various cities for decades. Heat mitigation technologies are typically used in urban areas to reduce cooling energy demand and improve the city’s thermal balance. The building’s construction and external weather conditions determine the relative benefits of heat rejection technologies. We evaluated the previously described eight scenarios (Table 2) to assess their impact on heat source strength and increase heat sinks’ cooling capacity. Figure 7 presents the cooling potential of the different mitigation scenarios compared to the base case. In this section, the maximum and minimum reductions of thermal properties compared to the base case are presented for each mitigation technology; the values are summarized in Table 8.

In addition, the ambient temperature at 2-m above the ground level, the surface temperature, air temperature (3D variable measured at 850 hPa), roof surface temperature, and urban canopy temperature were calculated. Additionally, Table 9 presents the reduction in 2-m ambient temperature and surface temperature for each scenario; the 24-h, daytime, and nighttime averages.

3.2.1 Cool roofs and cooling potential

Cool roof strategies were evaluated using a sensitivity study framework for the heat mitigation cases of cool roofs with varying albedo fractions for roofs. The results showed that the maximum/minimum reduction in ambient temperature was 1.5/0.41 °C, 3.6/0.69 °C, and 1.1/0.16 °C for cool roofs A, B, and C, respectively

(Fig. 8). For cool roof-A, B, and C, the maximum/minimum surface temperature reduced by 4.1/0.55 °C, 7.6/0.96 °C, and 2.9/0.24 °C, respectively. Furthermore, for those same cool roofs, the maximum/minimum air temperature was reduced by 0.66/0.22 °C, 1.8/0.38 °C, and 0.4/0.07 °C, respectively. While, for cool roof-A, cool roof-B, and cool roof-C, the model-generated maximum/minimum urban canopy temperature reduced by 5.1/0.54 °C, 10.1/0.93 °C, and 0.19/0.04 °C, respectively. The maximum/minimum roof surface temperature decreased by 12.7/0.89 °C, 20.7/1.6 °C, and 12.7/0.75 °C for cool roofs A, B, and C (Table 8). The temperature reduction is most significant for cool roof-B and lower in the case of strong warm air advection due to strong local convection. Cool roof-B reduces surface and ambient temperatures in core urban areas by as much as 1.6 °C and 1.1 °C at night.

3.2.2 Green roofs and cooling potential

The effectiveness of the proposed green roof techniques has been assessed based on their ability to reduce ambient air temperature, defined as the difference between average base case temperatures and the temperature of each green roof. Furthermore, the dynamically coupled green roof algorithm with four different layer structures calculated the green roofs’ temperature. WRF/SLUCM is used in conjunction with the green roof algorithm. To evaluate the cooling efficacy in an ambient environment for sensitivity tests, we used four green roof fractions:

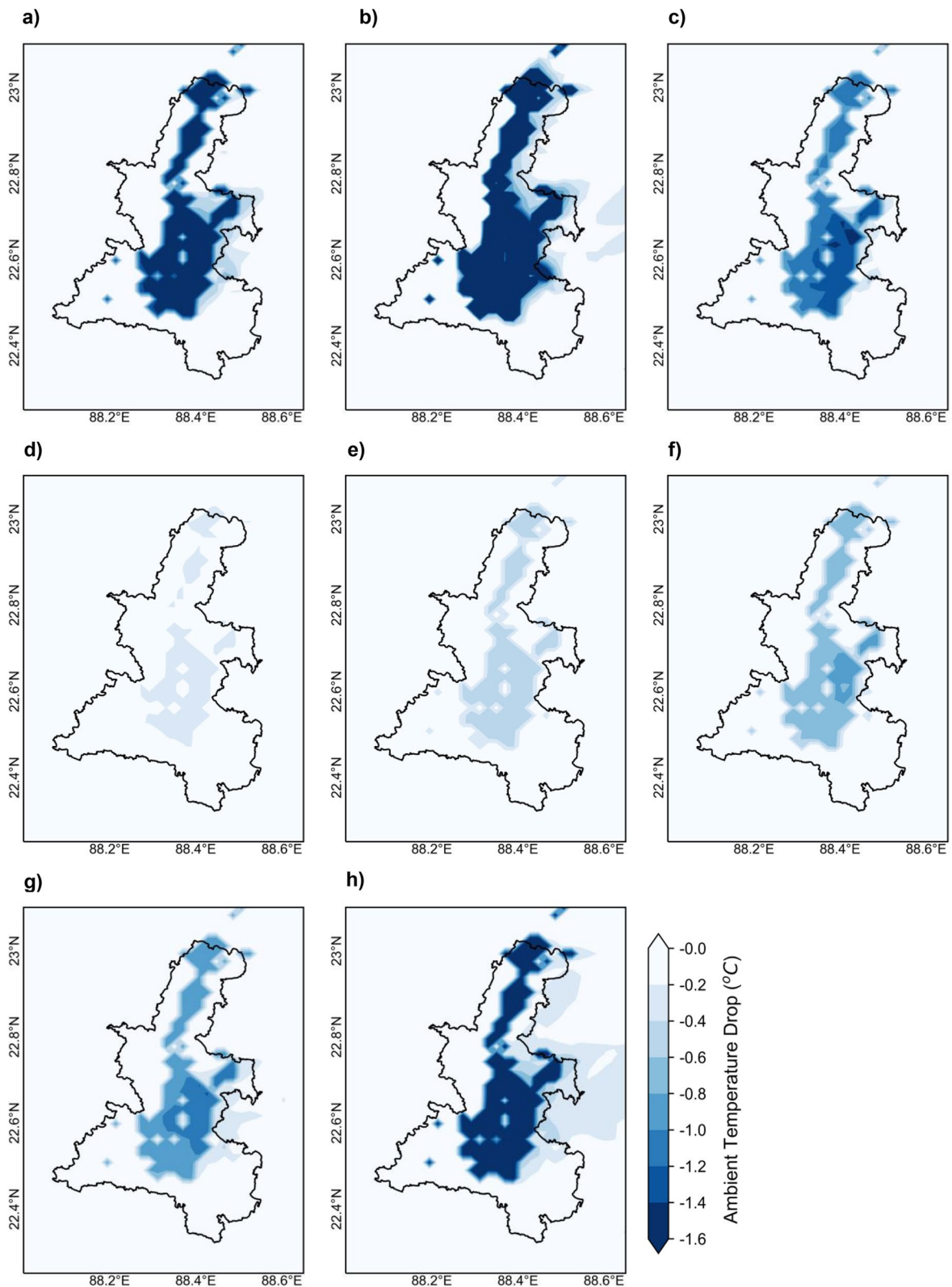


Fig. 8 Reduction in the ambient temperature as compared to the base case from heat mitigation technologies for **a** cool roof-A, **b** cool roof-B, **c** cool roof-C, **d** green roof-A, **e** green roof-B, **f** green roof-C, **g** green roof-D, **h** cool city

Table 7 Maximum and Minimum heat flux reduction (scenario minus base case) for the different heat mitigation technologies. H is the sensible heat flux, E is the latent heat flux, G is the heat flux into the ground and R_n is the net radiative flux density to the surface

| Scenarios | Cool roof-A | Cool roof-B | Cool roof-C | Green roof-A | Green roof-B | Green roof-C | Green roof-D | Cool city |
|---------------------|-------------|-------------|-------------|--------------|--------------|--------------|--------------|-----------|
| H (Wm^{-2}) | | | | | | | | |
| 24-h avg | -60.7 | -87.6 | -42.0 | -10.2 | -20.4 | -30.4 | -40.5 | -59.7 |
| Day | -100.1 | -141.5 | -71.9 | -16.9 | -33.3 | -49.7 | -66.0 | -96.8 |
| Night | -15.8 | -26.7 | -7.5 | -2.9 | -5.9 | -8.7 | -11.9 | -17.7 |
| E (Wm^{-2}) | | | | | | | | |
| 24-h avg | -4.6 | -9.0 | -2.6 | 13.2 | 26.2 | 38.9 | 51.5 | 22.1 |
| Day | -7.6 | -15.4 | -4.4 | 24.1 | 48.0 | 71.5 | 94.7 | 41.3 |
| Night | -1.3 | -1.9 | -0.73 | 0.64 | 1.1 | 1.6 | 2.0 | -0.08 |
| G (Wm^{-2}) | | | | | | | | |
| 24-h avg | 9.0 | 16.4 | 2.2 | -0.49 | -1.1 | -1.7 | -2.8 | 6.6 |
| Day | 35.5 | 63.2 | 12.1 | 1.9 | 3.7 | 5.4 | 6.8 | 32.6 |
| Night | -24.0 | -41.7 | -10.3 | -3.5 | -7.1 | -10.8 | -15.0 | -25.9 |
| R_n (Wm^{-2}) | | | | | | | | |
| 24-h avg | -74.3 | -113.1 | -46.7 | 3.4 | 6.9 | 10.2 | 13.8 | -44.2 |
| Day | -143.2 | -220.1 | -88.4 | 5.5 | 11.0 | 16.4 | 21.9 | -88.1 |
| Night | 6.9 | 13.1 | 2.1 | 1.2 | 2.4 | 3.6 | 5.1 | 8.1 |

25%, 50%, 75%, and 100% of each roof. The simulations with different green roof fractions show that substituting conventional roofs (base case) for 100% green roofs improves ambient cooling efficacy. The results showed that the maximum/minimum reduction in ambient temperature was 0.2/0.04 °C, 0.4/0.09 °C, 0.6/0.15 °C, and 0.9/0.3 °C for green roofs A, B, C, and D, respectively (Fig. 8). For green roof-A, B, C, and D, the surface temperature was reduced by 0.6/0.07 °C, 1.2/0.1 °C, 1.9/0.2 °C, and 2.5/1.2 °C, respectively. For those same green roofs, the maximum/minimum air temperature was reduced by 0.1/0.01 °C, 0.2/0.02 °C, 0.4/0.05 °C, and 0.5/0.1 °C, respectively. For green roof-A, B, C, and D, the maximum/minimum urban canopy temperature

was reduced by 0.1/0.01 °C, 0.1/0.01 °C, 0.2/0.02 °C, and 0.2/0.03 °C, respectively. Interestingly, due to synoptic weather variations and a lack of significant evapotranspiration, 100% of green roofs did not report sufficient canopy temperature reduction. For green roof-A, green roof-B, green roof-C, and green roof-D, the roof surface temperature decreased by 12.3/0.8 °C, 12.3/0.8 °C, 12.2/1.1 °C, and 12.2/1.14 °C, respectively (Table 7).

In other words, with 100% coverage of the green fraction, average roof temperatures dropped by 5.4 °C. Temperatures decreased linearly for the 25%, 50%, and 75% green roof scenarios, corresponding to an average of 5.2 °C, 5.3 °C, and 5.3 °C decreases, respectively (Fig. 9). The simulations are based on uniform green roof

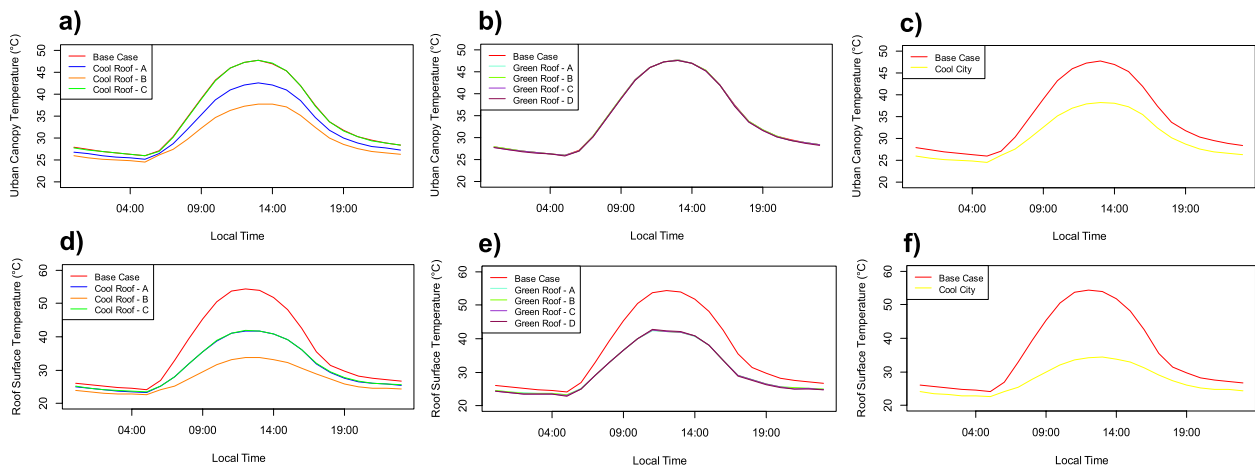


Fig. 9 Comparison of simulated urban canopy (a-c) and roof surface temperature (d-f) with the base scenario for different heat mitigation strategies

Table 8 Temperature reduction (scenario minus base case) for the different heat mitigation technologies. T_{amb} : 2 m-ambient temperature (°C), T_{surf} : Surface temperature (°C), T_{air} : Air temperature, T_{roof} : Roof surface temperature (°C), T_{canopy} : urban canopy temperature (°C)

| Scenarios | ΔT_{amb} | | ΔT_{surf} | | ΔT_{air} | | ΔT_{roof} | | ΔT_{canopy} | |
|--------------|------------------|-------|-------------------|-------|------------------|-------|-------------------|-------|---------------------|-------|
| | Max | Min | Max | Min | Max | Min | Max | Min | Max | Min |
| Cool roof-A | -1.5 | -0.41 | -4.1 | -0.55 | -0.66 | -0.22 | -12.7 | -0.89 | -5.1 | -0.54 |
| Cool roof-B | -3.6 | -0.69 | -7.6 | -0.96 | -1.8 | -0.38 | -20.7 | -1.6 | -10.1 | -0.93 |
| Cool roof-C | -1.1 | -0.16 | -2.9 | -0.24 | -0.4 | -0.07 | -12.7 | -0.75 | -0.19 | -0.04 |
| Green roof-A | -0.2 | -0.04 | -0.6 | -0.07 | -0.1 | -0.01 | -12.3 | -0.8 | -0.1 | -0.01 |
| Green roof-B | -0.4 | -0.09 | -1.2 | -0.1 | -0.2 | -0.02 | -12.3 | -0.8 | -0.1 | -0.01 |
| Green roof-C | -0.6 | -0.15 | -1.9 | -0.2 | -0.4 | -0.05 | -12.2 | -1.1 | -0.2 | -0.02 |
| Green roof-D | -0.9 | -0.3 | -2.5 | -1.2 | -0.5 | -0.1 | -12.2 | -1.14 | -0.2 | -0.03 |
| Cool city | -1.4 | -0.4 | -3.8 | -0.6 | -0.7 | -0.2 | -20.3 | -1.5 | -9.4 | -0.9 |

strategies in which each has a green roof cover of 25%, 50%, 75%, or 100%. The desired level of green roof percentage partitioned between conventional and green roofs is not physically possible for WRF/urban modeling. As a result, the current study did not test the effects of green roof patches on different building roof levels on the ambient thermal environment. The changes in ambient air temperature observed through 100% green roof strategies are negligible compared to the base case (Fig. 8).

The daytime and nighttime averages of each green roof scenario with similar meteorological conditions also present the diurnal profile of temperature reduction. During the day, the ambient temperature is reduced by 0.7 °C due to the 100% green roofing during peak hour (14:00 LT) and 0.4 °C at night (Table 9). Furthermore, the reduction of daytime roof surface temperature varied by adding a green roof fraction ranging from 25 to 100% during peak daytime (Fig. 9). Because of evapotranspirative cooling, the daytime surface temperature of a green roof is significantly lower than that of a conventional roof. The nighttime surface temperature on the green roof is also lower, but the differences between roofs are less pronounced. Furthermore, different urban physics from the urban core to the adjacent mixed urban surface significantly influence the thermal balance of the heterogeneous urban surface. It should be noted that local urbanization, anthropogenic heating, and local convection all influence air temperature, resulting in turbulence and uniform air warming.

3.2.3 Cool city and cooling potential

The experiment with combinations of urban greenery systems and reflective technologies reveals that the mitigation potential from combining different strategies and technologies (e.g., greenery and reflective materials) is greater than the sum of each technology’s contributions

(Santamouris et al., 2016). Therefore, we tested a single scenario for a combined case in the study. The maximum and minimum reductions in ambient, surface, air, canopy, and roof surface temperature were 1.4/0.4 °C, 3.8/0.6 °C, 0.7/0.2 °C, 9.4/0.9 °C, and 20.3/1.5 °C, respectively (Table 8). Compared to the experiment’s corresponding performance involving only reflective materials, the combined use of greenery and reflective materials reduces maximum temperatures by 1.4 °C, while the corresponding average temperature drop is 1 °C.

The cool city scenario’s daytime and nighttime averages also show the diurnal profile of temperature reduction. The average ambient and surface temperature reduction during the day is about 1.1 °C and 2.7 °C, respectively (Table 9). Furthermore, the reduction of daytime roof surface temperature constantly changed by increasing albedo fractions with the green roof at around 12 °C during peak daytime (Fig. 9). In cool city scenarios; the nighttime cooling efficacy is approximately 4.9 °C lower than daytime cooling efficacy. However, when some of these mitigation strategies are combined, the results are not as good as when used individually. It is also assumed that heat mitigation measures can be cost-effective when used in tandem. This combination of measures can reduce energy consumption, and anthropogenic emissions, improve decarbonization and reduce carbon sinking over rooftops and the urban atmosphere. Ultimately, these strategies reduce anthropogenic air pollution at the city scale. The findings demonstrate that the mitigation and cooling potential of the cool roof-B are less significant and can only contribute marginally to temperature reduction in the urban environment when compared with roof temperature versus ambient temperature (Fig. 10). However, if significant evaporation is continued with reflective materials, the cost of combined strategies could be high. Nevertheless, combined albedo/rooftop

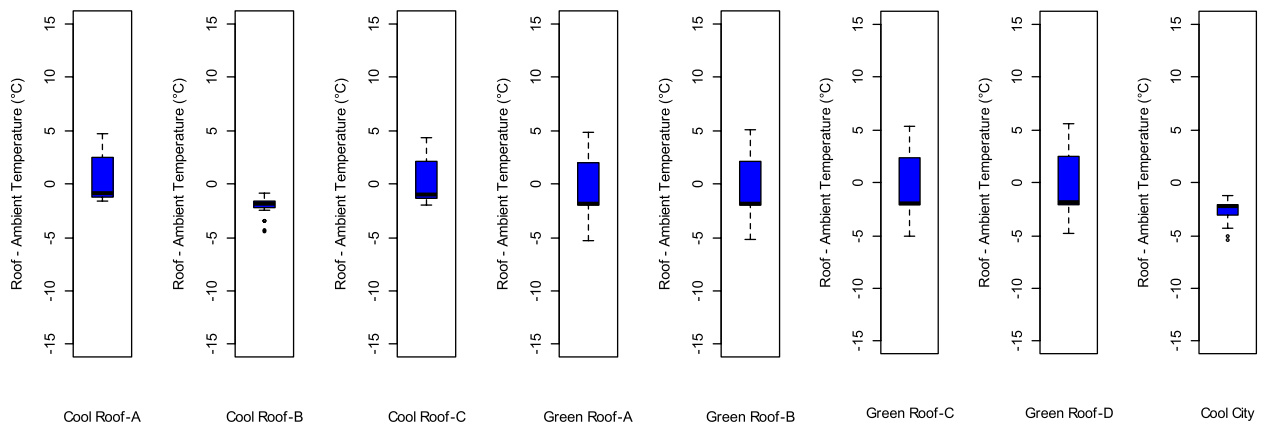


Fig. 10 Showing the standardized distribution of temperature differences between the roof and ambient temperature for a diurnal scale of each heat mitigation strategy

Table 9 The reduction of 2-m ambient temperature T_{amb} (°C) and surface temperature T_{surf} (°C) for each scenario minus base case average over the urban area. The values are separated into 24-h averages, the daytime and the nighttime

| Scenarios | ΔT_{amb} (°C) | | | ΔT_{surf} (°C) | | |
|--------------|-----------------------|-----------------------|-------------------------|------------------------|-----------------------|-------------------------|
| | 24-h avg | Daytime (05:00–17:00) | Nighttime (18:00–04:00) | 24-h avg | Daytime (05:00–17:00) | Nighttime (18:00–04:00) |
| Cool roof-A | -0.9 | -1.1 | -0.6 | -1.9 | -2.8 | -0.9 |
| Cool roof-B | -1.7 | -2.4 | -1.1 | -3.3 | -4.9 | -1.6 |
| Cool roof-C | -0.5 | -0.7 | -0.3 | -1.2 | -1.9 | -0.4 |
| Green roof-A | -0.1 | -0.2 | -0.1 | -0.3 | -0.4 | -0.1 |
| Green roof-B | -0.3 | -0.3 | -0.2 | -0.6 | -0.8 | -0.3 |
| Green roof-C | -0.4 | -0.5 | -0.3 | -0.9 | -1.3 | -0.4 |
| Green roof-D | -0.5 | -0.7 | -0.4 | -1.2 | -1.7 | -0.6 |
| Cool city | -0.9 | -1.1 | -0.7 | -1.9 | -2.7 | -1.0 |

cooling strategies could mitigate or reverse the summertime heat island effect.

On a clear summer day (39.2 °C), a standardized distribution of roof surface temperatures for different open roof surfaces (cool roofs, green roofs, cool city) with that of ambient air temperature is noted (Fig. 10). The results show that a reflective, cool roof surface can maintain excellent thermal performance. Compared to other roofs, the cool roof-B maintains a reduction of sub-ambient temperature of 3.5 °C throughout the day. The intensity of heat reduction is high during extreme solar energy and is open to the city’s conditions.

For each experiment, we plotted the results of ambient temperature versus surface temperature (Fig. 11). Except for cool roof-B, the results show a strong correlation between surface and ambient temperatures. Moreover, there was a significant difference in temperature between cool roof-B and the others. This result is consistent with a negative correlation between the base case and cool

roof-B differences. The results also indicated that the roof surface remained consistently below the ambient temperature throughout the simulation period, resulting in diurnal negative sensible heat flux released into the urban environment.

3.2.4 Efficacy of mitigation approaches

For quantitative comparison of different heat mitigation strategies, it is helpful to articulate the temperature reduction ($\Delta T_{max,min}$) of the ambient environment as a result of a specific heat mitigation strategy relative to a change in some property of the urban fabric (Rosenfeld et al., 1995). This efficiency is outlined in Eq. (9):

$$E_m = \frac{\Delta T_{max,min}}{\Delta(\rho)} \tag{9}$$

where $\Delta(\rho)$ is the change in a property, such as the albedo or green roof fraction. Thus, the efficiency is essentially

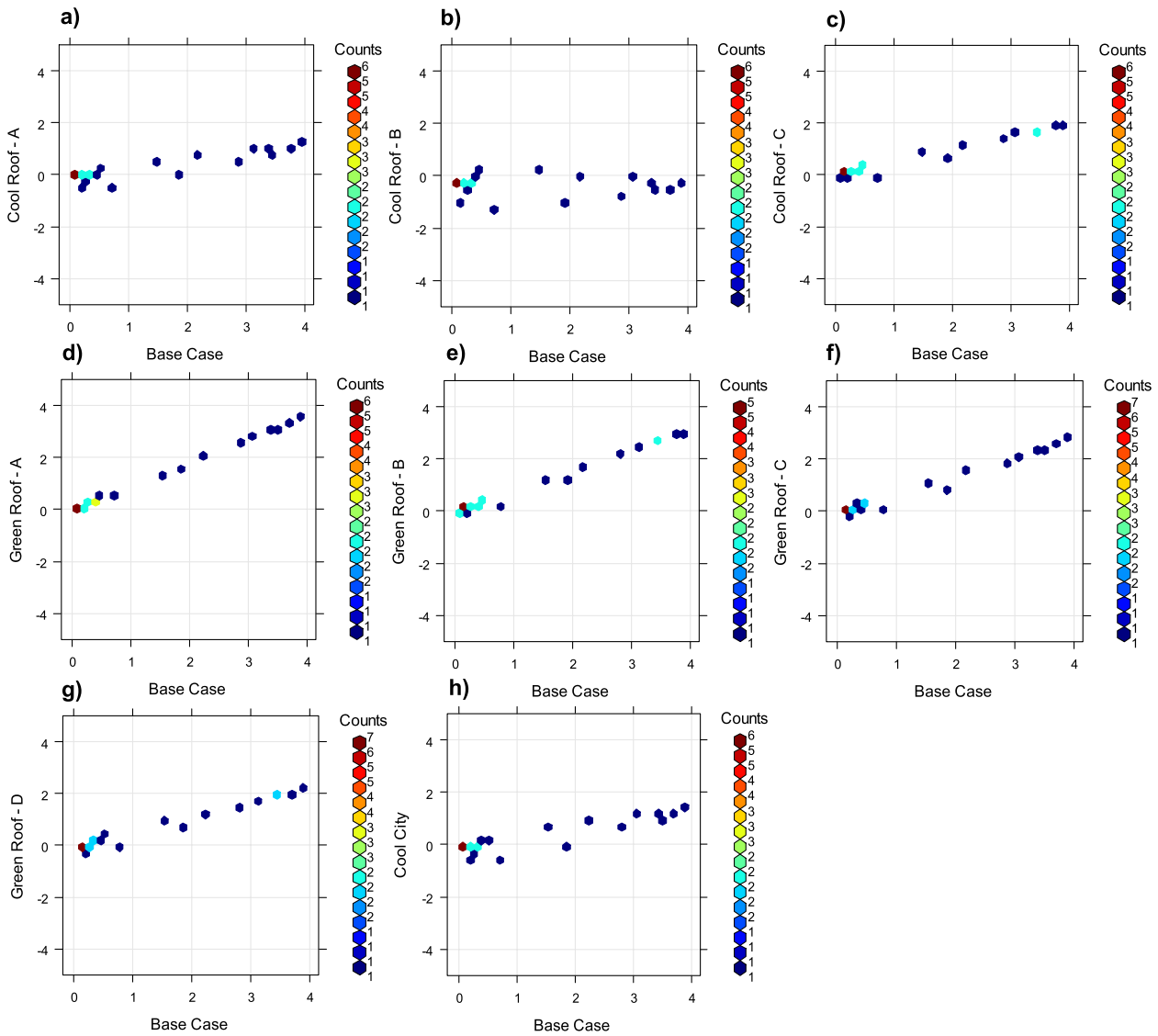


Fig. 11 The differences in temperature between the ambient air and the surface for base case scenario and mitigation scenarios **a-c** cool roof-A, B, and C; **d-g** green roof-A, B, C, and D; and **h** cool city on a typical day. The counts bar indicates the range of temperature scale (minimum to maximum), with each count designating a color and its related temperature values. Cool roof-B is the most effective mitigation strategy, reduced up to 1–2 °C

the gradient of the temperature change in relation to the property change. The numerical values for efficacy are determined through simulation at the city-scale rather than at the building level (Takebayashi & Moriyama, 2007). Also, each property parameter was normalized to compare heat mitigation strategies quantitatively. Given the various ranges available for $\Delta(p)$ it is also useful to express Eq. (9) in a non-dimensional form (Gui et al., 2007) as:

$$E_{m(nd)} = \frac{\Delta T_{max,min}}{\Delta(P)} \left[\frac{P_{ref}}{T_{ref}} \right] \quad (10)$$

where P_{ref} and T_{ref} are reference values for the property and temperature, respectively.

These dimensional and non-dimensional heat mitigation effectiveness for the three different strategies are presented in Table 10 and compared with the base case (with $T_{ref}=39.2/25.1$ °C, $\alpha_{ref}=0.2$, and $GR_{ref}=0$). When compared to green roofs and cool city strategies, the relative effects of competing urban heat mitigation strategies for cool roof-B are high, as increasing the albedo is proportional to decreasing temperatures. In the case of green roofs, it is noted that they are undervalued in strategies because they would almost always necessitate

Table 10 Dimensional and non-dimensional heat mitigation effectiveness for the strategies compared with the base case ($T_{ref} = 39.2/25.1$ °C, $\alpha_{ref} = 0.2$, and $GR_{ref} = 0$)

| Mitigation approach | Change in property | Average change in property | Temperature decrease (°C) | | Temperature gradient | | Dimensionless temperature gradient | |
|---------------------|------------------------|----------------------------|---------------------------|-----------|---|---|---|---|
| | | | T_{max} | T_{min} | $\left(\frac{\Delta T_{max}}{\Delta(P)}\right)$ | $\left(\frac{\Delta T_{min}}{\Delta(P)}\right)$ | $\frac{\Delta T_{max}}{\Delta(P)} \left(\frac{P_{ref}}{T_{ref}}\right)$ | $\frac{\Delta T_{min}}{\Delta(P)} \left(\frac{P_{ref}}{T_{ref}}\right)$ |
| Cool roof-A | Roof _{0,65} | 0.37 | -1.5 | -0.41 | 4.1 | 1.1 | 0.04 | 0.02 |
| | Wall _{0,20} | | | | | | | |
| | Ground _{0,20} | | | | | | | |
| Cool roof-B | Roof _{0,85} | 0.57 | -3.6 | -0.69 | 6.3 | 1.2 | 0.09 | 0.03 |
| | Wall _{0,20} | | | | | | | |
| | Ground _{0,20} | | | | | | | |
| Cool roof-C | Roof _{0,55} | 0.45 | -1.1 | -0.16 | 2.4 | 0.35 | 0.03 | 0.01 |
| | Wall _{0,20} | | | | | | | |
| | Ground _{0,20} | | | | | | | |
| Green roof-A | Roof _{0,25} | - | -0.20 | -0.04 | 0.79 | 0.12 | 0.01 | 0.002 |
| Green roof-B | Roof _{0,50} | - | -0.41 | -0.09 | 0.83 | 0.19 | 0.01 | 0.004 |
| Green roof-C | Roof _{0,50} | - | -0.64 | -0.12 | 0.86 | 0.20 | 0.02 | 0.01 |
| Green roof-D | Roof _{1,00} | - | -0.88 | -0.26 | 0.88 | 0.26 | 0.03 | 0.02 |
| Cool city | Roof _{1,00} | 0.68 | -1.4 | -0.41 | 2.1 | 0.60 | 0.04 | 0.02 |
| | Wall _{0,20} | | | | | | | |
| | Ground _{0,20} | | | | | | | |

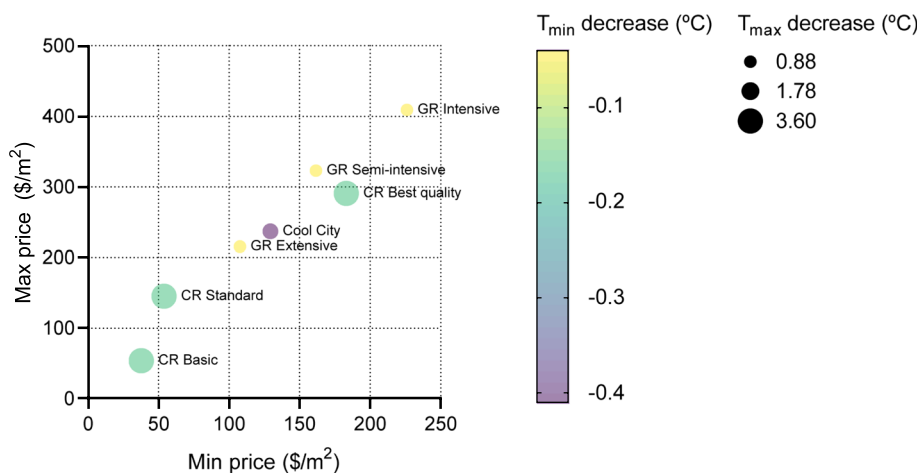


Fig. 12 Relationship between cost and reduction of the maximum ambient temperature and minimum ambient temperature. Estimations based on Table 3

structural adaptations of the buildings, while cool roofs typically do not.

As discussed in Section 2.2, the costs of various mitigation scenarios can vary based on the construction solution, location, and market prices. In this analysis, the relationship between cost per square meter and the potential temperature decrease was examined (Fig. 12). Since the relationship between scenarios and construction

solutions is not straightforward, we considered the maximum temperature reduction among all cool roof cases and the minimum temperature reduction among cool roof cases. The same approach was applied to green roofs. It is possible to find a cool roof with high reflectivity similar to Cool Roof-B scenario but at a lower price. Consequently, this estimation provides an overview of the cost per degree of cooling for all potential technologies.

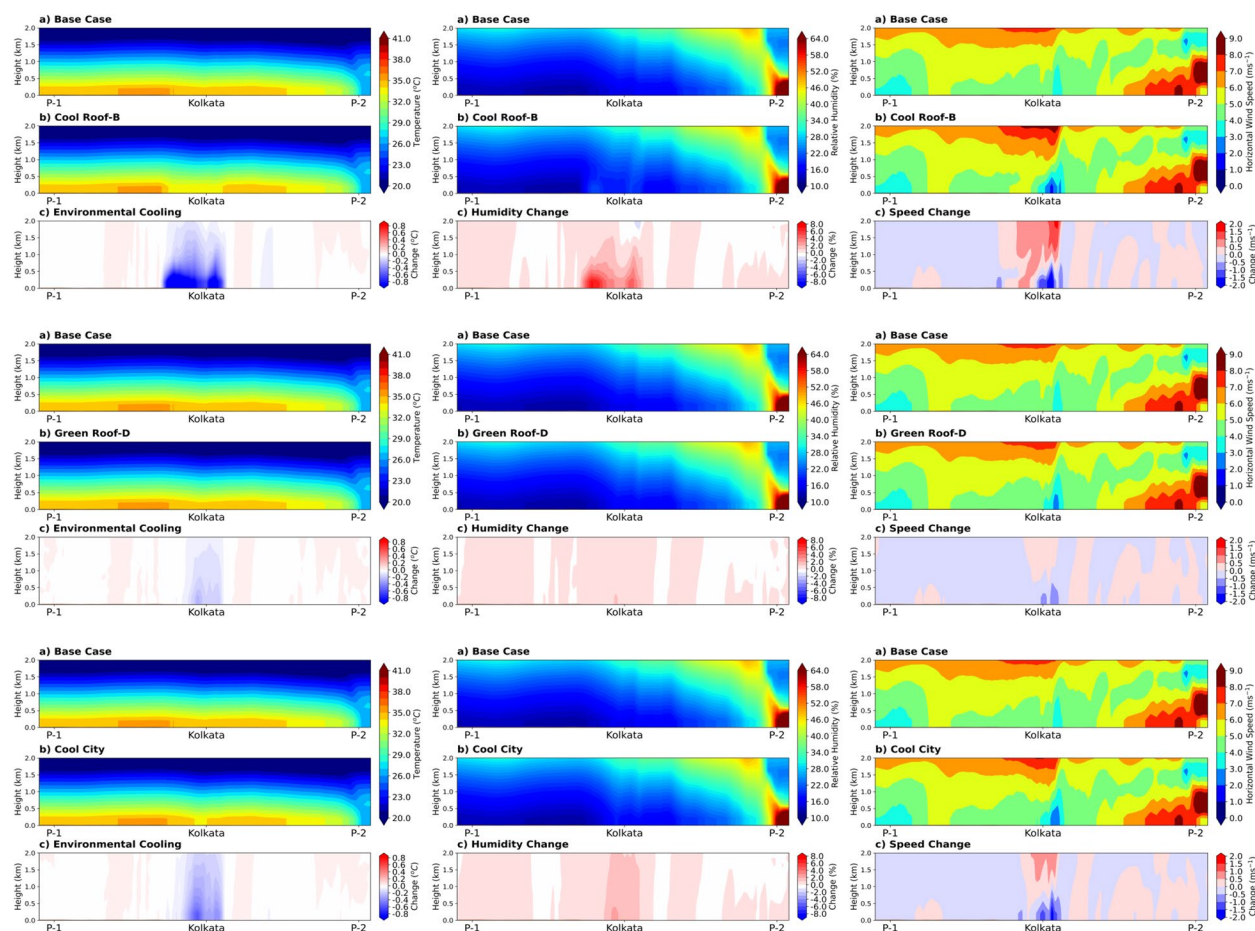


Fig. 13 Relative impacts of heat mitigation strategies on meteorological variables: temperature, relative humidity, and horizontal wind speed along points P-1 to P-2 as shown in Fig. 1

3.3 Urban cooling effects on the boundary layer structure

The changes in energy balance partitioning caused by increasing albedo and rooftop vegetation are greatly influenced by urban boundary layer structure. In the present study, we also demonstrated that both cool roof-B and green roofs would have more explicit urban cooling effects on the boundary layer structure. To demonstrate the effects of albedo and rooftop vegetation on the boundary layer, the peak time of changes in the vertical profile of temperature, horizontal wind speed, and relative humidity was investigated by subtracting the selected mitigation strategies, namely cool roof-B, green roof-D, and cool city, from the base case (Fig. 13).

During the day, the vertical temperature reduced within the lower atmosphere, but the degree of environmental cooling varies depending on the mitigation potential. Because of the increased albedo and emissivity, cool roof-B has the best environmental cooling. However, the maximum temperature drop of 0.9 °C was reported close to the ground. Reduced vertical mixing of

momentum flux may cause a decrease in horizontal wind speed. For cool roof-B, green roof-D, and cool city, the maximum vertical mixing is confined within 1 km of the lower atmosphere, with an increase beyond 1 km during the day. The momentum transfer from the upper to the lower layers has been reduced due to urban cooling strategies. Because of the lower-level reduction in vertical mixing, upper airflow with higher wind speed is less entrained into lower-level air with lower wind speed beyond 1 km during the day. As a result, in each experiment, wind speeds in the upper atmospheres over the city domain were reduced to a small degree. For Kolkata region, River Hooghly flows north to south, dividing the study area into eastern and western halves. The river contributes to a cooling effect on the higher ambient air temperatures, lowering the temperature from 1 °C to 2 °C during the day. However, due to the dense development of buildings along the river bank, the cooling effect does not extend beyond 30 m from the river and is negligible at 40 m (Chatterjee et al., 2016, 2019). The mitigation

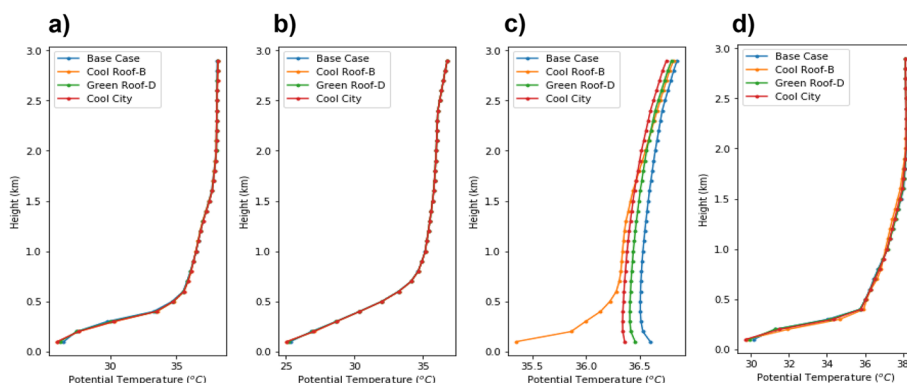


Fig. 14 Vertical distribution of potential temperature for different mitigation strategies during different times: **a** 00:00 LT **b** 06:00 LT, **c** 12:00 LT, and **d** 18:00 LT. Results show that the convective boundary layer was prominently developed during peak hour for base case (unmitigated scenarios)

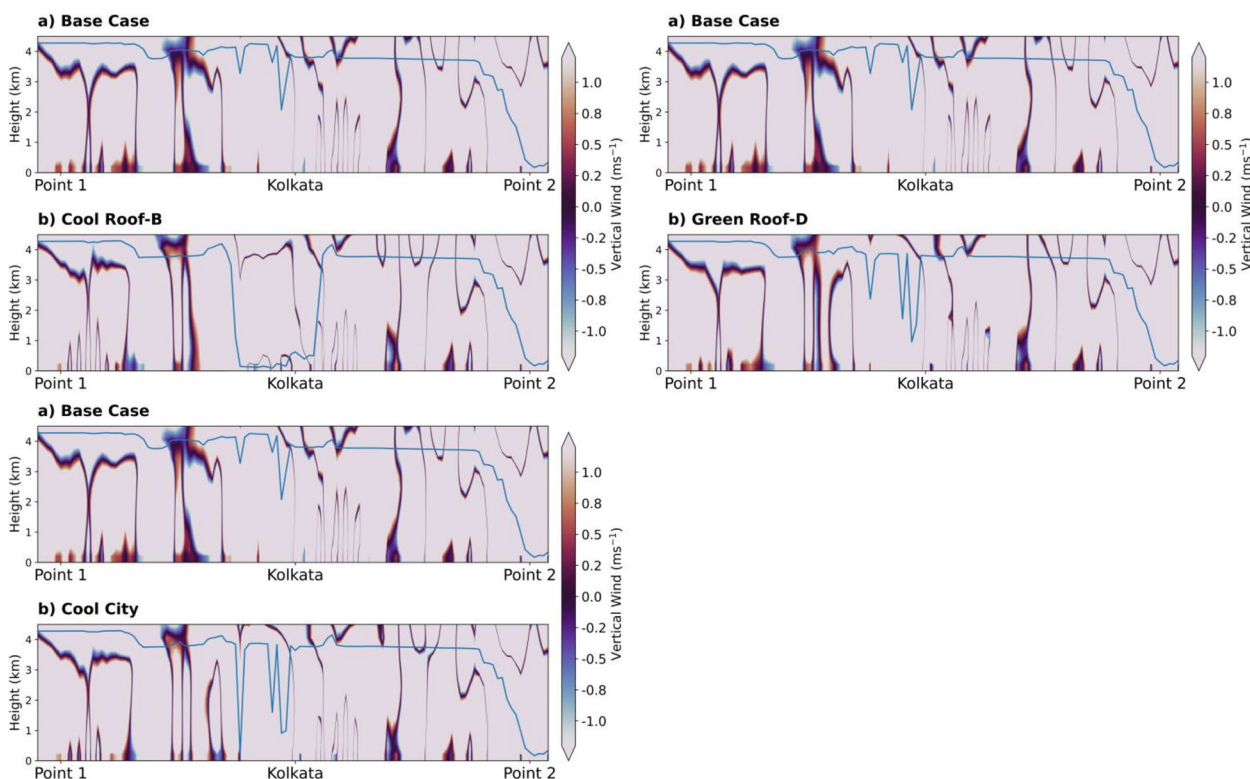


Fig. 15 Vertical wind and planetary boundary layer (blue line) along points P-1 and P-2 for peak hour (02:00 LT), for cool roof-B, green roof-D, and cool city, above the base case for comparison

potential of the strategies varies significantly due to synoptic atmospheric conditions. When wind speeds are high during the day, using reflective materials, green fraction on rooftops, and their combination results in higher temperature reduction.

The river-urban breeze is largely due to thermal gradient. By cooling the urban area, a reduction in the horizontal wind speeds was also noted. During the day, the green roof’s relative humidity was lower close to the

ground due to the low evaporation rate and light wind speeds. The relative humidity values increased for cool roofs due to temperature reductions associated with lower saturation vapor and advection of moist cool air from suburban areas.

The effects of urban cooling on boundary layer stability can be assessed using potential temperature (for a diurnal cycle (Fig. 14)). Compared to a cool roof, a green roof and cool city in the lower atmosphere, the convective

boundary layer developed the fastest and gradually deepened during peak hours (Feng et al., 2021). The effect of vertical mixing on wind speed and PBL height has been investigated (Fig. 15). The urban heat caused vertical mixing over the urban domain due to the higher sensible heat. However, urban heat mitigation techniques can reduce sensible heat or increase latent heat for the city's thermal management. The results indicate that PBL height was lower due to the cool roof-B scenario's higher reflectivity and decreased vertical mixing. As a result of this effect, there was less vertical convective mixing and a lower PBL height. In other words, the PBL contracts at night due to decreased rising thermals from the surface (Khan et al., 2022a, 2022b). In the base case, the PBL has a higher thickness of up to 2 km, whereas the green and cool roof scenarios can yield a PBL that is less than 1 km. Because of higher surface roughness and more significant shear, horizontal convective rolls are expected within the convective boundary layer; their major axes are aligned with the mean boundary layer wind-shear vector. Convective rolls were significantly weaker for cool roof-B than for green roof and cool city. It was caused primarily by thinner vertical wind updrafts and thicker downdrafts over the urban domain. For cool roof-B, weak vertical winds, less intense horizontal convective rolls, and lower horizontal velocity in the lower atmosphere (lower to 0.5 km) may contribute to increased cloud cover and air stagnation near the surface and longer withholding times of ground level pollutants released in the urban surface layer (Khan et al., 2023b).

4 Discussion

This research has studied the effect of cool roofs, green roofs, and a combined scenario (cool city) as heat mitigation technologies in a tropical urban environment. For the proposed mitigation cases, simulation results for Kolkata showed that increasing the albedo through cool materials can reduce the city's average maximum ambient temperature by 1.7 and 3.6 °C, depending on the cool roof's albedo. On the other hand, the maximum reduction in ambient temperature achieved by installing green roofs and cool cities was 0.2–0.9 °C, and 1.4 °C, respectively (Fig. 7). As a result, green roofs and cool cities were unable to achieve such a significant reduction in ambient temperature when compared to a cool roof for humid atmosphere during a typical summer day and less evapotranspiration. To provide a broader relevance of these results we summarize similar results for different locations as reported in the literature (Table 11).

The benefits of specific energy solutions depend on the local climate, rooftop greening design, and, most importantly, the characteristics of a specific building. The results showed that latent heat processes and heat

distribution primarily provide heat transfer benefits in green roofs and that system performance is higher in dry climates than in humid climates like Kolkata. More downward solar radiation governs the performance of green roofs. These radiations are converted to evapotranspiration, redistributing heat throughout the urban environment. The heat storage capacity of the roof surface increases with additional soil layers, lowering the roof surface temperature. Net radiation increased as albedo decreased from conventional to green roofs, resulting in a warm environment on the canopy layer and surrounding environment. As a result, green roofs are ineffective at mitigating urban heat in densely populated areas.

Nevertheless, green roofs are useful as they potentially reduce the inside temperature of residential buildings during peak summer days by shading, evapotranspiration, and insulation against incoming solar energy when compared to ambient air temperature. Meanwhile, during sunny days, the roofs act as a windshield, reducing the cooling energy demand of buildings. However, the effectiveness of a green roof during cold periods is not as notable as it is during summer days. Green roofs protect the ceiling from scorching shortwave radiation and extreme heat fluctuations. Green roofs can also reduce energy demand in various climatic conditions. Although reduction varies greatly depending on the climate, building function, type of green roof, and building insulation level.

In the areas of the city with highest temperatures, which also coincided to be regions of high-intensity residential, the reduction of temperatures for the ambient, surface, roof, and canopy was simulated by comparing all green roof scenarios. The results show the most significant temperature reduction from 25 to 100% green roofs. Furthermore, the mitigation potential of all four green roof strategies differ across areas of high-density residential areas, demonstrating a strong relationship between urban cooling potential and spatial location (Fig. 16). The findings from previous studies on the mitigation potential of green roofs (Chen et al., 2009; Ng et al., 2012) align with the results from current study. Overall, our result indicates a modest to insignificant performance of green roofs. When the ratio of building height to street width (aspect) exceeds 1, the urban cooling benefits showed reduction.

As seen in Fig. 16, cool roofs have a much higher mitigation potential for urban cooling and reducing building energy demands during peak hours (Santamouris, 2012). In our case, the peak sensible fluxes compared with the base case are 250 Wm⁻² and 115 Wm⁻² for cool roof B and green roof D. A study reported that during the day, the peak sensible fluxes from the cool and green roofs were close to 153 Wm⁻² and 361 Wm⁻², respectively

Table 11 Cool roof and green roof strategies and their effectiveness in the literature

| Cool roof strategies | | | |
|---------------------------------|--|--------------------------------------|-------------------------------|
| Cities (Country) | Albedo fraction | Temperature reduction | References |
| Montreal (Canada) | Roof: 0.45 Wall: 0.40 Road: 0.25 | 0.7 °C | (Touchaei et al., 2016) |
| Rome (Italy) | Roof: 0.65 Wall: 0.60 Road: 0.45 | 4 °C | (Morini et al., 2018) |
| Madrid (Spain) | Roof: 0.45 Road: 0.40 | 1.5–2 °C | (Salamanca et al., 2012) |
| Chicago (USA) | Roof: 0.85 | 3.22 °C | (Sharma et al., 2016) |
| Sacramento (USA) | Roof: 0.65 Wall: 0.60 Road: 0.45 | 2.37 °C | (Jandaghian & Akbari, 2018) |
| Houston (USA) | Roof: 0.65 Wall: 0.60 Road: 0.45 | 2.68 °C | |
| Chicago Metropolitan Area (USA) | Roof: 0.65 Wall: 0.60 Road: 0.45 | 1.76 °C | |
| Sydney (Australia) | All: 0.1–0.6 Road: 0.1–0.6 Roof: 0.2–0.7 | 0.6–3 °C 0.4–1.4 °C 0.1–0.6 °C | (Santamouris et al., 2018) |
| Phoenix (USA) | Roof: 0.75 | 0.5 °C | (Salamanca et al., 2016) |
| West Midlands (USA) | Roof: 0.70 | 0.5 °C | (Macintyre & Heaviside, 2019) |
| Stuttgart (Germany) | Roof: 0.70 | 1.2 °C | (Fallmann et al., 2016) |
| California (USA) | Roof: 0.85 | 0.9 °C | (Vahmani et al., 2016) |
| Los Angeles (USA) | Roof: 0.3 | 0.2 °C | (Taleghani et al., 2016) |
| Los Angeles (USA) | Average: 0.26 | 3.0 °C | (Rosenfeld et al., 1995) |
| Los Angeles (USA) | Roof: 0.50 | 1.5 °C | (Rosenfeld et al., 1998) |
| Atlanta (USA) | Average: 0.45 | 2.5 °C | (Zhou & Shepherd, 2010) |
| Houston (USA) | Roof: 0.30 Wall: 0.30 Pavement: 0.2 | 3.5 °C | (Taha, 2008) |
| New York (USA) | Average: 0.50 | 0.5 °C | (Lynn et al., 2009) |
| Green roof strategies | | | |
| Cities (Country) | Green fraction | Temperature reduction | References |
| Chicago (USA) | 25%—100% | 0.84—3.41 °C | (Sharma et al., 2016) |
| Sydney (Australia) | 100% | 0.75—1.5 °C | (Ma et al., 2018) |
| Sydney (Australia) | 100% | 0.5 °C | (Santamouris et al., 2018) |
| Los Angeles (USA) | 100% | 0.2 °C | (Taleghani et al., 2016) |

(Scherba et al., 2011). Over 24 h, the average sensible heat fluxes were 20 Wm^{-2} and 2 Wm^{-2} . During the summer, the maximum sensible fluxes for both cool and green roofs were roughly equal, while the daily sensible heat flux for green roofs was twice that of reflective roofs (Santamouris, 2012). An evaluation of the mitigation scenario with black roof revealed that cool and green roofs reduce the maximum sensible heat flux by more than 70%, while total daily sensible heat is reduced by 80% and 52%, respectively, when allowing for a cool or green roof (Santamouris, 2012; Takebayashi & Moriyama, 2007).

Prior findings, summarized in Table 11, provide useful information, but these findings only provide a gross perspective. It should also be noted that more precise characterization of the urban albedo fraction results in a more localized representation of the urban thermal environment. The simulation results show that changing the albedo reduces the ambient temperature during the day and at night. Most of the data is based on simulation studies that use the mesoscale modeling approach, but significant data is available from current experimental studies. The initial and boundary conditions used for

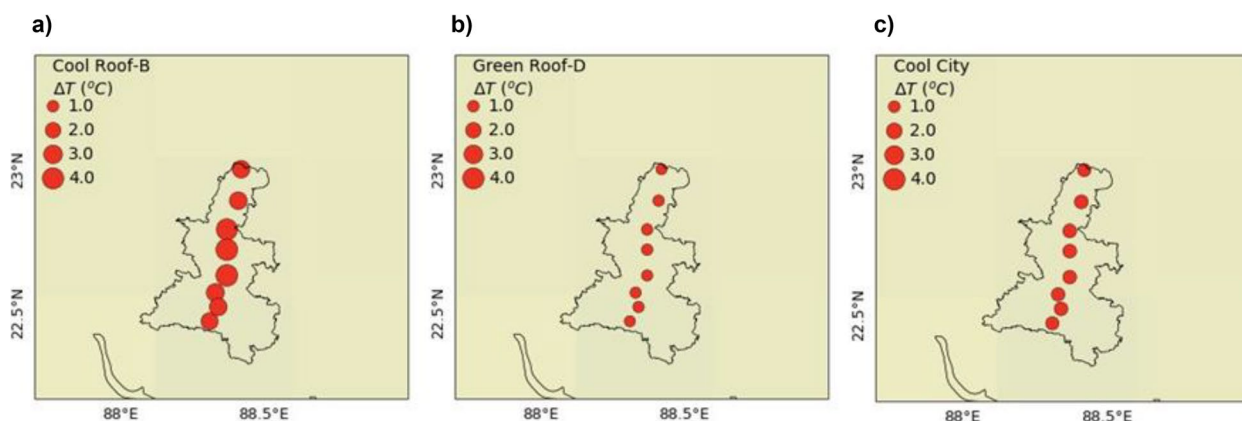


Fig. 16 Comparison with the base scenario for different heat mitigation strategies and their strong connection between cooling potential and spatial locations for **a** cool roof-B, **b** green roof-D, and **c** cool city

various numerical evaluations for each studied city in different climate zones are quite different. It is unclear in the literature which studies have used localized model input parameters for simulations. Moreover, it was also found that the reported studies provided model inputs in various non-comparative formats, and lack of localized information needs to be reported in future studies to achieve better transferability of results (Santamouris, 2014).

As regards to the urban heat mitigation, increasing the albedo fraction offered promising results, lowering the maximum ambient temperature in high-intensity areas by up to 3.6 °C during the day for a cool roof-B scenario. The changes in the diurnal scale are also noted, with averages of 2.4 °C during the daytime and 1.1 °C at nighttime (Table 9). Cool roofs A and C are less effective than cool roof B, as their albedo is lower. The temperature is reduced by increased albedo throughout the day and at night. As a result, the decrease in thermal storage of urban surfaces has a significant impact.

The relationship between increasing albedo and decreasing ambient temperature is roughly linear (Santamouris, 2012). The highest decrease of the roof surface temperature is close to 3.2 °C per 0.1 rises in albedo, while the highest decrease of the peak ambient temperature is close to 0.6 °C in high-intensity residential areas. When only cool roofs and pavements are considered, the expected depression rate of the average urban surface temperature ranges from 0.2 °C to 1.3 °C per 0.1 increase in roof, wall, and ground (road) albedo, with a mean value close to 0.8 °C.

Climatic seasonality influences the mitigation potential of rooftop technologies. Cool roofs lower ambient air temperatures and produce less heating of the surrounding air because they reflect more incoming solar energy. It is also noted that cool roofs controlled by energy distribution factors that encode the efficacies of

the surface energy balance component are dissipating heat. The findings indicate that painting a white roof is more effective when it has less water-holding capacity and less thermal admittance and is in areas with more solar radiation, less rainfall, and low wind speeds. Overall, reflective roofs are advantageous in warm climates with low humidity levels, whereas green roofs are advantageous in temperate and cold climates and vice versa in humid climates. The important variable is the ambient temperature, which determines the amount of sensible heat released by roofs, walls, and grounds (Santamouris, 2012). Convective heat flow is a direct function of temperature variation between the roof and the ambient temperature, but it varies synoptically and seasonally. The expected climatic impact and mitigation potential of reflective or green roofs installed in high-rise buildings are very limited, as building height and street width are essential factors in determining cooling potential through energy exchange.

Weathering is a significant concern for reflective and vegetative roofs in tropical climates. Roof reflectance degrades over time because of dust accumulation, ultraviolet radiation, microbial growth, acid rain, moisture penetration and condensation, wind, and biomass accumulation. The primary cause of reflectance loss in roadside buildings due to vehicular combustions and black carbon particles, also known as soot particles. Well-irrigated green roofs of the extensive type with a high leaf area index ($LAI > 1.5$) may have an equivalent mitigation potential to cool roofs with an initial albedo of around or greater than 0.7 (Bretz & Akbari, 1997).

Increasing the roof albedo fraction in tropical settings reduces heat ingress through the roof surface (Garg et al., 2016). When converting the conventional roof into a cool roof, an examination should be

carried out to find suitable heat reflective materials and waterproofing membranes. Cool roofs with high solar reflectance and thermal emittance stay cool in the sun during peak solar hours (Akbari & Levinson, 2008). As a result, the higher outflow of longwave radiation creates less inflow radiation and low heat gain over the urban domain, causing the low surface temperature on the building facet and a lower outflow of thermal radiation into the lower atmosphere (Akbari & Matthews, 2012).

Specific to this study domain, the proposed cool roofs provide the most cooling efficacy in Kolkata, where summers are hot and winters are dry, but they can raise energy costs during the winter due to reduced beneficial heat gains. A study already pointed out that under very reflective and emissive scenarios, the maximum decrease of net radiation at peak hour was 354.9 Wm^{-2} ; therefore, choosing a scenario with lower albedo values for walls and ground would be more beneficial during the winter period (Khan et al., 2021a). Therefore, materials must be chosen based on their competence, efficiency, cost-effectiveness, technical, maintenance, and environmental considerations (Akbari & Levinson, 2008; Akbari et al., 2005).

The cost of the roofing material and mitigation approach is an important component of this study, and more localized studies considering the mitigative potential and corresponding costs can be undertaken.

5 Conclusions

For possible urban heat mitigation solutions, we investigated the use of different types of green and cool roofs and evaluated them for two typical pre-monsoon hot summer days (in April 2020) using the WRF/SLUCM system. The increased fraction of albedo or rooftop vegetation resulted in changes to the surface energy balance of roofs, walls, and grounds (road) for urban grid cells. As a result, the thermal parameters of the city domain (surface temperature, ambient temperature, air temperature, roof surface temperature, and urban canopy temperature) changed significantly.

A novelty of this study is that we studied the impact of different mitigation strategies on the city's temperature (roof, ambient, surface, urban canyon), relative humidity, horizontal wind speed, and on the heat fluxes. We conducted a sensitivity analysis by varying the albedo values of the cool roofs and the green fraction of the green roofs, finally we assessed the combination of the best case for each (cool-city). Moreover, the properties of the walls and roads remain unchanged, the only parameters that change are the roof's properties. As a result, we can compare under the same street condition the roofs' impact on the city level. The results showed that green roofs

and cool cities were unable to achieve such a significant reduction in ambient temperature when compared to a cool roof for humid atmosphere during a typical summer day and less evapotranspiration. Cool roofs lower ambient air temperatures and produce less heating of the surrounding air because they reflect more incoming solar energy. As a result, they are more effective at improving urban thermal balance and lowering building cooling energy demands.

Another important novelty of this study is to place the cooling mitigation performance in the context of the cost relative to cooling efficiency. This analysis should be developed for more regional studies and would provide useful information for city planners and infrastructure design. Generally, green roofs are typically more expensive to install than cool roofs, but also have a longer expected life. Nevertheless, a 0.3 m (0.5–0.2 m) green roof has a significant structural load (400 kg/m^2), which must be anticipated in the building structures. Furthermore, adding such a load to most of older buildings is generally not possible. So, the thermal load as well as structural and costs of the mitigation strategies need to be better documented.

In the present study, the average UHI intensity varies between $1.8 \text{ }^\circ\text{C}$ and $2.1 \text{ }^\circ\text{C}$ day and night. When using several mitigation strategies, the maximum ambient temperature fell by $3.6 \text{ }^\circ\text{C}$, $0.9 \text{ }^\circ\text{C}$, and $1.4 \text{ }^\circ\text{C}$ for cool roof-B (85% albedo), green roof-D (100% rooftop vegetation), and a combination of both (cool-city). The best-performing mitigation scenarios and their combinations could reduce peak UHI intensity while increasing diurnal thermal comfort. Compared to green roofs, cool roofs are more effective at improving urban thermal balance and lowering building cooling energy demands. Because of the lower level of evapotranspiration, the effectiveness of green roofs is low. Green roofs act as an energy distributor over urban areas when the evaporative cooling process is high. The cool-city outperforms green roofs by including vegetation on the roof with higher albedo. We demonstrated that both cool and green roofs would reduce winds and exaggerate lower atmospheric thermodynamics during peak hours, such as low-level vertical mixing, decreased planetary boundary layer height, and weakening horizontal convective rolls. These meteorological changes in the lower atmosphere need to be considered for impact of air pollution and public health exposure.

The scarcity of data sets (necessary for model parameterization) captured for the rapidly expanding tropical cities, most located in developing countries, is a major impediment to conducting research. Furthermore, more climatological parameters must be tested to ensure that green or cool roofs have the desired

effects on local convection. On the other hand, the fraction of albedo or green roof is a single fraction that we applied uniformly to all urban grid cells. Therefore, future simulations must have finer-grained control (e.g., per gridcell) to set a specific fraction of albedo or vegetation for the roofs, walls, and grounds (road) in only selected areas of the city to be cool roofs or green roofs. Furthermore, experimental and numerical evaluation should encourage a holistic heat mitigation plan for the rapidly growing cities. At the city scale, this holistic approach could aid in the reduction of urban heat-induced costs for peak electricity demand, energy consumption, indoor thermal comfort, heat-related mortality, and morbidity, vulnerability, and survivability. The results provided in this study could assist with information on the urban cooling potential of heat mitigation as an engineering and meteorological strategy for lowering thermal anomaly and building energy use in different cities.

The high albedo and emissivity can create contrast and reflective glare in the urban atmosphere during peak temperatures. Material refinements are required to diffuse the reflectance to avoid contrast and glare effects without increasing solar absorption. Researchers may be interested in balancing the three spectral elements of materials to develop climate-friendly, highly reflective cool materials: very high albedo, atmospheric window absorption level, and atmospheric radiation absorption and reflection. The absorption of atmospheric radiation within the city domain is heavily influenced by local energy balance, convection, atmospheric water, synoptic weather conditions, and building morphologies.

Acknowledgements

This research was made possible with meteorological data support from the Weather Kolkata, Kolkata Municipal Corporation (KMC), Kolkata. Dev Niyogi acknowledges support from the U.S. National Science Foundation, NASA Interdisciplinary Sciences Program, and the University of Texas at Austin.

Authors' contributions

Conceptualization: Ansar Khan. Formal analysis: Ansar Khan, Samiran Khorat, Quang-Van Doan. Funding acquisition: Dev Niyogi. Investigation: Rupali Khatun, Laura Carlosena. Methodology: Ansar Khan, Samiran Khorat. Software: Ansar Khan, Samiran Khorat, Quang-Van Doan. Writing – original draft: Ansar Khan. Supervision: Hashem Akbari, Mattheos Santamouris, Dev Niyogi. Writing – review and editing: Laura Carlosena, Debashish Das, Rafiq Hamdi, Sk Mohammad Aziz, Hashem Akbari, Mattheos Santamouris, Dev Niyogi.

Funding

This research was made possible with meteorological data support from the Weather Kolkata, Kolkata Municipal Corporation, Kolkata. Dev Niyogi acknowledges financial support from US NOAA-NIHHS (NA21OAR4310146; Program Manager: Hunter Jones); the NASA Interdisciplinary Sciences program (80NSSC20K1262 and 80NSSC20K1268), the U.S. National Science Foundation (1835739, 2051110, and 2228205), and the University of Texas at Austin for William Stamps Farish Chair funds and the Bridging Barriers/Planet Texas 2050 initiative.

Availability of data and materials

The data that support the findings of this study are available from the corresponding author upon reasonable request. The source code of the WRF

model, Version 4.0 used in this paper can be downloaded from <https://www2.mmm.ucar.edu/wrf/users/downloads.html>. Codes used to set up model simulations, analyze data, and create figures can be provided upon request from the corresponding author.

Declarations

Competing interests

The authors declare that they do not have any known competing financial interests or personal relationships that could appear to have influenced the work reported in this paper.

Author details

¹Department of Geography, Lalbaba College, University of Calcutta, Kolkata, India. ²Engineering Department, Public University of Navarre (UPNA), Arrosadia Campus, 31006 Pamplona, Spain. ³School of Environmental Studies, Jadavpur University, Kolkata, India. ⁴Department of Architecture, Jadavpur University, Kolkata, India. ⁵Centre for Computational Sciences, University of Tsukuba, Tsukuba, Japan. ⁶Royal Meteorological Institute of Belgium, Brussels, Belgium. ⁷Department of Chemistry, Narajole Raj College, Vidyasagar University, Midnapore, India. ⁸Heat Island Group, Department of Building, Civil, and Environmental Engineering, Concordia University, Montreal, Canada. ⁹Department of Built Environment, University of New South Wales, Sydney, Australia. ¹⁰Department of Geological Sciences, Jackson School of Geosciences, Department of Civil, Architectural, and Environmental Engineering, Cockrell School of Engineering, University of Texas, Austin, TX, USA.

Received: 23 March 2023 Revised: 9 July 2023 Accepted: 12 July 2023

Published online: 04 August 2023

References

- Ahmedabad Municipal Corporation. (2019). *Ahmedabad heat action plan. Guide to extreme heat planning in Ahmedabad, India.* <https://www.nrcd.org/sites/default/files/ahmedabad-heat-action-plan-2018.pdf>
- Akbari, H., & Kolokotsa, D. (2016). Three decades of urban heat islands and mitigation technologies research. *Energy and Buildings*, 133, 834–842. <https://doi.org/10.1016/j.enbuild.2016.09.067>
- Akbari, H., & Levinson, R. (2008). Evolution of Cool-Roof Standards in the US. *Advances in Building Energy Research*, 2(1), 1–32. <https://doi.org/10.3763/aber.2008.0201>
- Akbari, H., & Matthews, H. D. (2012). Global cooling updates: Reflective roofs and pavements. *Energy and Buildings*, 55, 2–6. <https://doi.org/10.1016/j.enbuild.2012.02.055>
- Akbari, H., Levinson, R., & Rainer, L. (2005). Monitoring the energy-use effects of cool roofs on California commercial buildings. *Energy and Buildings*, 37(10), 1007–1016. <https://doi.org/10.1016/j.enbuild.2004.11.013>
- Alapaty, K., Pleim, J. E., Raman, S., Niyogi, D. S., & Byun, D. W. (1997). Simulation of atmospheric boundary layer processes using local- and nonlocal-closure schemes. *Journal of Applied Meteorology and Climatology*, 36(3), 214–233. [https://doi.org/10.1175/1520-0450\(1997\)036%3C0214:SOABLP%3e2.0.CO;2](https://doi.org/10.1175/1520-0450(1997)036%3C0214:SOABLP%3e2.0.CO;2)
- Alapaty, K., Seaman, N. L., Niyogi, D. S., & Hanna, A. F. (2001). Assimilating surface data to improve the accuracy of atmospheric boundary layer simulations. *Journal of Applied Meteorology (1988–2005)*, 40(11), 2068–2082
- Ao, X., Grimmond, C. S. B., Liu, D., Han, Z., Hu, P., Wang, Y., Zhen, X., & Tan, J. (2016). Radiation fluxes in a business district of Shanghai, China. *Journal of Applied Meteorology and Climatology*, 55(11), 2451–2468. <https://doi.org/10.1175/JAMC-D-16-0082.1>
- Aslam, B., Maqsoom, A., Khalid, N., Ullah, F., & Sepasgozar, S. (2021). Urban overheating assessment through prediction of surface temperatures: A case study of Karachi Pakistan. *ISPRS International Journal of Geo-Information*, 10(8), 539. <https://doi.org/10.3390/ijgi10080539>
- Bixler, R. P., Coudert, M., Richter, S. M., Jones, J. M., Llanes Pulido, C., Akhavan, N., Bartos, M., Passalacqua, P., & Niyogi, D. (2022). Reflexive co-production for urban resilience: Guiding framework and experiences from Austin, Texas. *Frontiers in Sustainable Cities*, 4, 1015630. <https://www.frontiersin.org/articles/10.3389/frsc.2022.1015630>

- Bogoslovskij, V. N. (1982). *Wärmetechnische Grundlagen der Heizungs-*. Verlag für Bauwesen.
- Bretz, S. E., & Akbari, H. (1997). Long-term performance of high-albedo roof coatings. *Energy and Buildings*, 25(2), 159–167. [https://doi.org/10.1016/S0378-7788\(96\)01005-5](https://doi.org/10.1016/S0378-7788(96)01005-5)
- Bretz, S., Akbari, H., Rosenfeld, A., & Taha, H. (1992). *Implementation of solar-reflective surfaces: Materials and utility programs* (LBL-32467). Lawrence Berkeley National Lab. (LBNL). <https://doi.org/10.2172/10172670>
- Carlosena, L., Andueza, Á., Torres, L., Irulegi, O., Hernández-Minguillón, R. J., Sevilla, J., & Santamouris, M. (2021). Experimental development and testing of low-cost scalable radiative cooling materials for building applications. *Solar Energy Materials and Solar Cells*, 230, 111209. <https://doi.org/10.1016/j.solmat.2021.111209>
- Chakraborty, T., Das, D., Hamdi, R., Khan, A., & Niyogi, D. (2023). Large-Scale Urban Heating and Pollution Domes over the Indian Subcontinent. *Remote Sensing*, 15(10), Article 10. <https://doi.org/10.3390/rs15102681>
- Chatterjee, S., Khan, A., Akbari, H., & Wang, Y. (2016). Monotonic trends in spatio-temporal distribution and concentration of monsoon precipitation (1901–2002), West Bengal, India. *Atmospheric Research*, 182, 54–75. <https://doi.org/10.1016/j.atmosres.2016.07.010>
- Chatterjee, S., Khan, A., Dinda, A., Mithun, S., Khatun, R., Akbari, H., Kusaka, H., Mitra, C., Bhatti, S. S., Van Doan, Q., & Wang, Y. (2019). Simulating micro-scale thermal interactions in different building environments for mitigating urban heat islands. *Science of the Total Environment*, 663, 610–631. <https://doi.org/10.1016/j.scitotenv.2019.01.299>
- Chen, H., Ooka, R., Huang, H., & Tsuchiya, T. (2009). Study on mitigation measures for outdoor thermal environment on present urban blocks in Tokyo using coupled simulation. *Building and Environment*, 44(11), 2290–2299. <https://doi.org/10.1016/j.buildenv.2009.03.012>
- Chen, F., Kusaka, H., Bornstein, R., Ching, J., Grimmond, C. S. B., Grossman-Clarke, S., Loridan, T., Manning, K. W., Martilli, A., Miao, S., Sailor, D., Salamanca, F. P., Taha, H., Tewari, M., Wang, X., Wyszogrodzki, A. A., & Zhang, C. (2011). The integrated WRF/urban modelling system: Development, evaluation, and applications to urban environmental problems. *International Journal of Climatology*, 31(2), 273–288. <https://doi.org/10.1002/joc.2158>
- Chen, F., & Dudhia, J. (2001). Coupling an advanced land surface–hydrology model with the Penn State–NCAR MM5 modeling system. Part I: Model implementation and sensitivity. *Monthly Weather Review*, 129(4), 569–585. [https://doi.org/10.1175/1520-0493\(2001\)129<0569:CAALSH>2.0.CO;2](https://doi.org/10.1175/1520-0493(2001)129<0569:CAALSH>2.0.CO;2)
- Chew, L. W., Liu, X., Li, X.-X., & Norford, L. K. (2021). Interaction between heat wave and urban heat island: A case study in a tropical coastal city, Singapore. *Atmospheric Research*, 247, 105134. <https://doi.org/10.1016/j.atmosres.2020.105134>
- CRRC Roof Directory. (n.d.). Retrieved May 26, 2023, from <https://coolroofs.org/directory/roof>
- Dai, T.-Y., Radhakrishnan, P., Nweye, K., Estrada, R., Niyogi, D., & Nagy, Z. (2023). Analyzing the impact of COVID-19 on the electricity demand in Austin, TX using an ensemble-model based counterfactual and 400,000 smart meters. *Computational Urban Science*, 3(1), 20. <https://doi.org/10.1007/s43762-023-00095-w>
- Davies, F., Middleton, D. R., & Bozier, K. E. (2007). Urban air pollution modelling and measurements of boundary layer height. *Atmospheric Environment*, 41(19), 4040–4049. <https://doi.org/10.1016/j.atmosenv.2007.01.015>
- de Munck, C., Lemonsu, A., Masson, V., Le Bras, J., & Bonhomme, M. (2018). Evaluating the impacts of greening scenarios on thermal comfort and energy and water consumptions for adapting Paris city to climate change. *Urban Climate*, 23, 260–286. <https://doi.org/10.1016/j.uclim.2017.01.003>
- Doan, Q.-V., Chen, F., Kusaka, H., Dipankar, A., Khan, A., Hamdi, R., Roth, M., & Niyogi, D. (2022). Increased Risk of Extreme Precipitation Over an Urban Agglomeration With Future Global Warming. *Earth's Future*, 10(6), e2021EF002563. <https://doi.org/10.1029/2021EF002563>
- Doulos, L., Santamouris, M., & Livada, I. (2004). Passive cooling of outdoor urban spaces The Role of Materials. *Solar Energy*, 77(2), 231–249. <https://doi.org/10.1016/j.solener.2004.04.005>
- Dudhia, J. (1989). Numerical study of convection observed during the winter monsoon experiment using a mesoscale two-dimensional model. *Journal of the Atmospheric Sciences*, 46(20), 3077–3107. [https://doi.org/10.1175/1520-0469\(1989\)046%3c3077:NSOCOD%3e2.0.CO;2](https://doi.org/10.1175/1520-0469(1989)046%3c3077:NSOCOD%3e2.0.CO;2)
- Fakhruddin, B., Kirsch-Wood, J., Niyogi, D., Guoqing, L., Murray, V., & Frolova, N. (2022). Harnessing risk-informed data for disaster and climate resilience. *Progress in Disaster Science*, 16, 100254. <https://doi.org/10.1016/j.pdisas.2022.100254>
- Fallmann, J., Forkel, R., & Emeis, S. (2016). Secondary effects of urban heat island mitigation measures on air quality. *Atmospheric Environment*, 125, 199–211. <https://doi.org/10.1016/j.atmosenv.2015.10.094>
- Feng, J., Khan, A., Doan, Q.-V., Gao, K., & Santamouris, M. (2021). The heat mitigation potential and climatic impact of super-cool broadband radiative coolers on a city scale. *Cell Reports Physical Science*, 2(7), 100485. <https://doi.org/10.1016/j.xcrp.2021.100485>
- Feng, J., Saliari, M., Gao, K., & Santamouris, M. (2022). On the cooling energy conservation potential of super cool roofs. *Energy and Buildings*, 264, 112076. <https://doi.org/10.1016/j.enbuild.2022.112076>
- Garg, V., Somal, S., Arumugam, R., & Bhatia, A. (2016). Development for cool roof calculator for India. *Energy and Buildings*, 114, 136–142. <https://doi.org/10.1016/j.enbuild.2015.06.022>
- Garshasbi, S., Feng, J., Paolini, R., Jonathan Duverge, J., Bartesaghi-Koc, C., Arasteh, S., Khan, A., & Santamouris, M. (2023). On the energy impact of cool roofs in Australia. *Energy and Buildings*, 278, 112577. <https://doi.org/10.1016/j.enbuild.2022.112577>
- González-Torres, M., Pérez-Lombard, L., Coronel, J. F., Maestre, I. R., & Yan, D. (2022). A review on buildings energy information: Trends, end-uses, fuels and drivers. *Energy Reports*, 8, 626–637. <https://doi.org/10.1016/j.egy.2021.11.280>
- Gui, J., & (Gavin) Phelan, P. E., Kaloush, K. E., & Golden, J. S. (2007). Impact of pavement thermophysical properties on surface temperatures. *Journal of Materials in Civil Engineering*, 19(8), 683–690. [https://doi.org/10.1061/\(ASCE\)0899-1561\(2007\)19:8\(683\)](https://doi.org/10.1061/(ASCE)0899-1561(2007)19:8(683))
- Han, Y., Taylor, J. E., & Pisello, A. L. (2015). Toward mitigating urban heat island effects: Investigating the thermal-energy impact of bio-inspired retro-reflective building envelopes in dense urban settings. *Energy and Buildings*, 102, 380–389. <https://doi.org/10.1016/j.enbuild.2015.05.040>
- Houston, A. L., & Niyogi, D. (2007). The Sensitivity of Convective Initiation to the Lapse Rate of the Active Cloud-Bearing Layer. *Monthly Weather Review*, 135(9), 3013–3032. <https://doi.org/10.1175/MWR3449.1>
- Hu, J., Yang, Y., Zhou, Y., Zhang, T., Ma, Z., & Meng, X. (2022). Spatial patterns and temporal variations of footprint and intensity of surface urban heat island in 141 China cities. *Sustainable Cities and Society*, 77, 103585. <https://doi.org/10.1016/j.scs.2021.103585>
- Huang, K., Lee, X., Stone Jr., B., Knierel, J., Bell, M. L., & Seto, K. C. (2021). Persistent increases in nighttime heat stress from urban expansion despite heat island mitigation. *Journal of Geophysical Research: Atmospheres*, 126(4), e2020JD033831. <https://doi.org/10.1029/2020JD033831>
- Imran, H. M., Kala, J., Ng, A. W. M., & Muthukumar, S. (2018). Effectiveness of green and cool roofs in mitigating urban heat island effects during a heatwave event in the city of Melbourne in southeast Australia. *Journal of Cleaner Production*, 197, 393–405. <https://doi.org/10.1016/j.jclepro.2018.06.179>
- IPCC, 2018: Global Warming of 1.5°C. An IPCC Special Report on the impacts of global warming of 1.5°C above pre-industrial levels and related global greenhouse gas emission pathways, in the context of strengthening the global response to the threat of climate change, sustainable development, and efforts to eradicate poverty [Masson-Delmotte, V., P. Zhai, H.-O. Pörtner, D. Roberts, J. Skea, P.R. Shukla, A. Pirani, W. Moufouma-Okia, C. Péan, R. Pidcock, S. Connors, J.B.R. Matthews, Y. Chen, X. Zhou, M.I. Gomis, E. Lonnoy, T. Maycock, M. Tignor, and T. Waterfield (eds.)]. In Press.
- Jacobs, S. J., Gallant, A. J. E., Tapper, N. J., & Li, D. (2018). Use of cool roofs and vegetation to mitigate urban heat and improve human thermal stress in Melbourne, Australia. *Journal of Applied Meteorology and Climatology*, 57(8), 1747–1764. <https://doi.org/10.1175/JAMC-D-17-0243.1>
- Jain, M., Dimri, A. P., & Niyogi, D. (2016). Urban sprawl patterns and processes in Delhi from 1977 to 2014 based on remote sensing and spatial metrics approaches. *Earth Interactions*, 20(14), 1–29. <https://doi.org/10.1175/EI-D-15-0040.1>
- Jandaghian, Z., & Akbari, H. (2018). The effect of increasing surface Albedo on urban climate and air quality: A detailed study for Sacramento, Houston, and Chicago. *Climate*, 6(2), Article 2. <https://doi.org/10.3390/cli6020019>

- Kaginalkar, A., Kumar, S., Gargava, P., & Niyogi, D. (2021). Review of urban computing in air quality management as smart city service: An integrated IoT, AI, and cloud technology perspective. *Urban Climate*, 39, 100972. <https://doi.org/10.1016/j.uclim.2021.100972>
- Kain, J. S. (2004). The Kain-Fritsch convective parameterization: an update. *Journal of Applied Meteorology and Climatology*, 43(1), 170–181. [https://doi.org/10.1175/1520-0450\(2004\)043%3c0170:TKCPAU%3e2.0.CO;2](https://doi.org/10.1175/1520-0450(2004)043%3c0170:TKCPAU%3e2.0.CO;2)
- Khan, A., Akbari, H., Fiorito, F., Mithun, S., & Niyogi, D. (2022a). *Global urban heat island mitigation*. Elsevier. <https://www.sciencedirect.com/science/article/pii/B9780323855396010015>
- Khan, A., Carlosena, L., Feng, J., Khorat, S., Khatun, R., Doan, Q.-V., & Santamouris, M. (2022b). Optically modulated passive broadband daytime radiative cooling materials can cool cities in summer and heat cities in winter. *Sustainability*, 14(3), 1110. <https://doi.org/10.3390/su14031110>
- Khan, A., Carlosena, L., Khorat, S., Khatun, R., Doan, Q.-V., Feng, J., & Santamouris, M. (2021a). On the winter overcooling penalty of super cool photonic materials in cities. *Solar Energy Advances*, 1, 100009. <https://doi.org/10.1016/j.seja.2021.100009>
- Khan, A., Chatterjee, S., Akbari, H., Bhatti, S. S., Dinda, A., Mitra, C., Hong, H., & Doan, Q. V. (2019). Step-wise Land-class Elimination Approach for extracting mixed-type built-up areas of Kolkata megacity. *Geocarto International*, 34(5), 504–527. <https://doi.org/10.1080/10106049.2017.1408704>
- Khan, A., Chatterjee, S., Filho, W. L., Khatun, R., Dinda, A., & Minhas, A. (2020). City-scale Modeling of Urban Heat Islands for Kolkata. In W. Leal Filho, G. J. Nagy, M. Borga, P. D. Chávez Muñoz, & A. Magnuszewski (Eds.), *Climate Change, Hazards and Adaptation Options: Handling the Impacts of a Changing Climate* (pp. 89–133). Springer International Publishing. https://doi.org/10.1007/978-3-030-37425-9_5
- Khan, A., & Chatterjee, S. (2016). Numerical simulation of urban heat island intensity under urban–suburban surface and reference site in Kolkata, India. *Modeling Earth Systems and Environment*, 2(2), 71. <https://doi.org/10.1007/s40808-016-0119-5>
- Khan, A., Chatterjee, S., & Wang, Y. (2021b). *Urban heat island modeling for tropical climates*. Elsevier.
- Khan, A., Khorat, S., Doan, Q., Khatun, R., Das, D., Hamdi, R., Carlosena, L., Santamouris, M., Georgescu, M., & Niyogi, D. (2023a). Exploring the meteorological impacts of surface and rooftop heat mitigation strategies over a tropical City. *Journal of Geophysical Research: Atmospheres*, 128(8), e2022JD038099. <https://doi.org/10.1029/2022JD038099>
- Khan, A., Khorat, S., Doan, Q.-V., Khatun, R., Das, D., Hamdi, R., Carlosena, L., Santamouris, M., Georgescu, M., & Niyogi, D. (2023b). Exploring the meteorological impacts of surface and rooftop heat mitigation strategies over a tropical city. *Journal of Geophysical Research: Atmospheres*, n/a(n/a), e2022JD038099. <https://doi.org/10.1029/2022JD038099>
- Khan, A., Papazoglou, E. G., Cartalis, C., Philippopoulos, K., Vasilakopoulou, K., & Santamouris, M. (2022c). On the mitigation potential and urban climate impact of increased green infrastructures in a coastal mediterranean city. *Building and Environment*, 221, 109264. <https://doi.org/10.1016/j.buildenv.2022.109264>
- Knight, T., Price, S., Bowler, D., Hookway, A., King, S., Konno, K., & Richter, R. L. (2021). How effective is 'greening' of urban areas in reducing human exposure to ground-level ozone concentrations, UV exposure and the 'urban heat island effect'? An Updated Systematic Review. *Environmental Evidence*, 10(1), 12. <https://doi.org/10.1186/s13750-021-00226-y>
- Kolokotsa, D., Maravelaki-Kalaitzaki, P., Papantoniou, S., Vangeloglou, E., Saliari, M., Karlessi, T., & Santamouris, M. (2012). Development and analysis of mineral based coatings for buildings and urban structures. *Solar Energy*, 86(5), 1648–1659. Scopus. <https://doi.org/10.1016/j.solener.2012.02.032>
- Kusaka, H., Kondo, H., Kikegawa, Y., & Kimura, F. (2001). A simple single-layer urban canopy model for atmospheric models: comparison with multi-layer and slab models. *Boundary-Layer Meteorology*, 101(3), 329–358. <https://doi.org/10.1023/A:1019207923078>
- Li, D., & Bou-Zeid, E. (2013). Synergistic interactions between urban heat islands and heat waves: the impact in cities is larger than the sum of its parts. *Journal of Applied Meteorology and Climatology*, 52(9), 2051–2064. <https://doi.org/10.1175/JAMC-D-13-02.1>
- Li, D., Bou-Zeid, E., & Oppenheimer, M. (2014). The effectiveness of cool and green roofs as urban heat island mitigation strategies. *Environmental Research Letters*, 9(5), 055002. <https://doi.org/10.1088/1748-9326/9/5/055002>
- Lin, Y.-L., Farley, R. D., & Orville, H. D. (1983). Bulk parameterization of the snow field in a cloud model. *Journal of Applied Meteorology and Climatology*, 22(6), 1065–1092. [https://doi.org/10.1175/1520-0450\(1983\)022%3c1065:BPOTSF%3e2.0.CO;2](https://doi.org/10.1175/1520-0450(1983)022%3c1065:BPOTSF%3e2.0.CO;2)
- Liu, X., Li, X.-X., Harshan, S., Roth, M., & Velasco, E. (2017). Evaluation of an urban canopy model in a tropical city: The role of tree evapotranspiration. *Environmental Research Letters*, 12(9), 094008. <https://doi.org/10.1088/1748-9326/aa7ee7>
- Luckett, K. (2009). *Green roof construction and maintenance*. McGraw-Hill.
- Lynn, B. H., Carlson, T. N., Rosenzweig, C., Goldberg, R., Druyan, L., Cox, J., Gaffin, S., Parshall, L., & Civerolo, K. (2009). A modification to the NOAA LSM to simulate heat mitigation strategies in the New York City metropolitan area. *Journal of Applied Meteorology and Climatology*, 48(2), 199–216. <https://doi.org/10.1175/2008JAMC1774.1>
- Ma, S., Pitman, A., Yang, J., Carouge, C., Evans, J. P., Hart, M., & Green, D. (2018). Evaluating the effectiveness of mitigation options on heat stress for Sydney, Australia. *Journal of Applied Meteorology and Climatology*, 57(2), 209–220. <https://doi.org/10.1175/JAMC-D-17-0061.1>
- Macintyre, H. L., & Heaviside, C. (2019). Potential benefits of cool roofs in reducing heat-related mortality during heatwaves in a European city. *Environment International*, 127, 430–441. <https://doi.org/10.1016/j.envint.2019.02.065>
- Masson, V. (2006). Urban surface modeling and the meso-scale impact of cities. *Theoretical and Applied Climatology*, 84(1), 35–45. <https://doi.org/10.1007/s00704-005-0142-3>
- Matthews, T. K. R., Wilby, R. L., & Murphy, C. (2017). Communicating the deadly consequences of global warming for human heat stress. *Proceedings of the National Academy of Sciences*, 114(15), 3861–3866. <https://doi.org/10.1073/pnas.1617526114>
- Mellor, G. L., & Yamada, T. (1974). A hierarchy of turbulence closure models for planetary boundary layers. *Journal of the Atmospheric Sciences*, 31, 1791–1806. Scopus.
- Miao, S., Chen, F., LeMone, M. A., Tewari, M., Li, Q., & Wang, Y. (2009). An observational and modeling study of characteristics of urban heat island and boundary layer structures in Beijing. *Journal of Applied Meteorology and Climatology*, 48(3), 484–501. <https://doi.org/10.1175/2008JAMC1909.1>
- Mills, G., Stewart, I. D., & Niyogi, D. (2022). The origins of modern urban climate science: Reflections on 'A numerical model of the urban heat island'. *Progress in Physical Geography: Earth and Environment*, 46(4), 649–656. <https://doi.org/10.1177/03091333221107212>
- Mlawer, E. J., Taubman, S. J., Brown, P. D., Iacono, M. J., & Clough, S. A. (1997). Radiative transfer for inhomogeneous atmospheres: RRTM, a validated correlated-k model for the longwave. *Journal of Geophysical Research: Atmospheres*, 102(D14), 16663–16682. <https://doi.org/10.1029/97JD0237>
- Mohammed, A., Khan, A., & Santamouris, M. (2022). Numerical evaluation of enhanced green infrastructures for mitigating urban heat in a desert urban setting. *Building Simulation*. <https://doi.org/10.1007/s12273-022-0940-x>
- Mohammed, A., Khan, A., & Santamouris, M. (2021). On the mitigation potential and climatic impact of modified urban albedo on a subtropical desert city. *Building and Environment*, 206, 108276. <https://doi.org/10.1016/j.buildenv.2021.108276>
- Morini, E., Touchaei, A. G., Rossi, F., Cotana, F., & Akbari, H. (2018). Evaluation of albedo enhancement to mitigate impacts of urban heat island in Rome (Italy) using WRF meteorological model. *Urban Climate*, 24, 551–566. <https://doi.org/10.1016/j.uclim.2017.08.001>
- Mughal, M. O., Li, X.-X., Yin, T., Martilli, A., Brousse, O., Dissegna, M. A., & Norford, L. K. (2019). High-resolution, multilayer modeling of Singapore's urban climate incorporating local climate zones. *Journal of Geophysical Research: Atmospheres*, 124(14), 7764–7785. <https://doi.org/10.1029/2018JD029796>
- NCEP Central Operations. (n.d.). *NCEP Data Products GFS and GDAS*. NCEP Central Operations. <https://www.nco.ncep.noaa.gov/pmb/products/gfs/>
- Ng, E., Chen, L., Wang, Y., & Yuan, C. (2012). A study on the cooling effects of greening in a high-density city: An experience from Hong Kong. *Building and Environment*, 47, 256–271. <https://doi.org/10.1016/j.buildenv.2011.07.014>
- Nichol, J. E. (1996). High-resolution surface temperature patterns related to urban morphology in a tropical city: A satellite-based study. *Journal of*

- Applied Meteorology and Climatology*, 35(1), 135–146. [https://doi.org/10.1175/1520-0450\(1996\)035%3c0135:HRSTPR%3e2.0.CO;2](https://doi.org/10.1175/1520-0450(1996)035%3c0135:HRSTPR%3e2.0.CO;2)
- Niyogi, D. S., Raman, S., & Alapaty, K. (1999). Uncertainty in the specification of surface characteristics. Part ii: Hierarchy of interaction-explicit statistical analysis. *Boundary-Layer Meteorology*, 91(3), 341–366. <https://doi.org/10.1023/A:1002023724201>
- Niyogi, D., Pyle, P., Lei, M., Arya, S. P., Kishtawal, C. M., Shepherd, M., Chen, F., & Wolfe, B. (2011). Urban modification of thunderstorms: an observational storm climatology and model case study for the Indianapolis urban region. *Journal of Applied Meteorology and Climatology*, 50(5), 1129–1144. <https://doi.org/10.1175/2010JAMC1836.1>
- Niyogi, D., Holt, T., Zhong, S., Pyle, P. C., & Basara, J. (2006). Urban and land surface effects on the 30 July 2003 mesoscale convective system event observed in the southern Great Plains. *Journal of Geophysical Research: Atmospheres*, 111(D19). <https://doi.org/10.1029/2005JD006746>
- Niyogi, D., Subramanian, S., Mohanty, U. C., Kishtawal, C. M., Ghosh, S., Nair, U. S., Ek, M., & Rajeevan, M. (2018). The impact of land cover and land use change on the Indian monsoon region hydroclimate. In K. P. Vadrevu, T. Ohara, & C. Justice (Eds.), *Land-atmospheric research applications in South and Southeast Asia* (pp. 553–575). Springer International Publishing. https://doi.org/10.1007/978-3-319-67474-2_25
- Niyogi, D., Osuri, K. K., Busireddy, N. K. R., & Nadimpalli, R. (2020). Timing of rainfall occurrence altered by urban sprawl. *Urban Climate*, 33, 100643. <https://doi.org/10.1016/j.uclim.2020.100643>
- Oke, T. R. (1988). The urban energy balance. *Progress in Physical Geography: Earth and Environment*, 12(4), 471–508. <https://doi.org/10.1177/030913338801200401>
- Patel, P., Karmakar, S., Ghosh, S., Aliaga, D. G., & Niyogi, D. (2021). Impact of green roofs on heavy rainfall in tropical, coastal urban area. *Environmental Research Letters*, 16(7), 074051. <https://doi.org/10.1088/1748-9326/ac1011>
- Patel, P., Kalyanam, R., He, L., Aliaga, D., & Niyogi, D. (2023). Deep learning-based urban morphology for city-scale environmental modeling. *PNAS Nexus*, 2(3), pgad027. <https://doi.org/10.1093/pnasnexus/pgad027>
- Pleim, J. E. (2007). A combined local and nonlocal closure model for the atmospheric boundary layer. Part I: Model description and testing. *Journal of Applied Meteorology and Climatology*, 46(9), 1383–1395. <https://doi.org/10.1175/JAM2539.1>
- Qi, J., Ding, L., & Lim, S. (2020). Planning for cooler cities: A framework to support the selection of urban heat mitigation techniques. *Journal of Cleaner Production*, 122903. <https://doi.org/10.1016/j.jclepro.2020.122903>
- Ramamurthy, P., & Bou-Zeid, E. (2014). Contribution of impervious surfaces to urban evaporation. *Water Resources Research*, 50(4), 2889–2902. <https://doi.org/10.1002/2013WR013909>
- Ramamurthy, P., & Bou-Zeid, E. (2017). Heatwaves and urban heat islands: A comparative analysis of multiple cities. *Journal of Geophysical Research: Atmospheres*, 122(1), 168–178. <https://doi.org/10.1002/2016JD025357>
- Reagan, J. A., & Acklam, D. M. (1979). Solar reflectivity of common building materials and its influence on the roof heat gain of typical southwestern U.S.A. residences. *Energy and Buildings*, 2(3), 237–248. [https://doi.org/10.1016/0378-7788\(79\)90009-4](https://doi.org/10.1016/0378-7788(79)90009-4)
- Rigby, M., & Toumi, R. (2008). London air pollution climatology: Indirect evidence for urban boundary layer height and wind speed enhancement. *Atmospheric Environment*, 42(20), 4932–4947. <https://doi.org/10.1016/j.atmosenv.2008.02.031>
- Rosenfeld, A. H., Akbari, H., Bretz, S., Fishman, B. L., Kurn, D. M., Sailor, D., & Taha, H. (1995). Mitigation of urban heat islands: Materials, utility programs, updates. *Energy and Buildings*, 22(3), 255–265. [https://doi.org/10.1016/0378-7788\(95\)00927-P](https://doi.org/10.1016/0378-7788(95)00927-P)
- Rosenfeld, A. H., Akbari, H., Romm, J. J., & Pomerantz, M. (1998). Cool communities: Strategies for heat island mitigation and smog reduction. *Energy and Buildings*, 28(1), 51–62. [https://doi.org/10.1016/S0378-7788\(97\)00063-7](https://doi.org/10.1016/S0378-7788(97)00063-7)
- Roth, M. (2007). Review of urban climate research in (sub)tropical regions. *International Journal of Climatology*, 27(14), 1859–1873. <https://doi.org/10.1002/joc.1591>
- Salamanca, F., Martilli, A., & Yagüe, C. (2012). A numerical study of the Urban Heat Island over Madrid during the DESIREX (2008) campaign with WRF and an evaluation of simple mitigation strategies. *International Journal of Climatology*, 32(15), 2372–2386. <https://doi.org/10.1002/joc.3398>
- Salamanca, F., Georgescu, M., Mahalov, A., Moustauou, M., & Martilli, A. (2016). Citywide impacts of cool roof and rooftop solar photovoltaic deployment on near-surface air temperature and cooling energy demand. *Boundary-Layer Meteorology*, 161(1), 203–221. <https://doi.org/10.1007/s10546-016-0160-y>
- Santamouris, M. (2012). *Advances in passive cooling*. Routledge.
- Santamouris, M., & Feng, J. (2018). Recent progress in daytime radiative cooling: Is it the air conditioner of the future? *Buildings*, 8(12), 168. <https://doi.org/10.3390/buildings8120168>
- Santamouris, M., & Kolokotsa, D. (2016). *Urban climate mitigation techniques*. Routledge.
- Santamouris, M., Synnefa, A., Kolokotsa, D., Dimitriou, V., & Apostolakis, K. (2008). Passive cooling of the built environment—Use of innovative reflective materials to fight heat islands and decrease cooling needs. *International Journal of Low-Carbon Technologies*, 3(2), 71–82. <https://doi.org/10.1093/ijlct/3.2.71>
- Santamouris, M., Ding, L., Fiorito, F., Oldfield, P., Osmond, P., Paolini, R., Prasad, D., & Synnefa, A. (2016). Passive and active cooling for the outdoor built environment – Analysis and assessment of the cooling potential of mitigation technologies using performance data from 220 large scale projects. *Solar Energy*, 154, 14–33. <https://doi.org/10.1016/j.solener.2016.12.006>
- Santamouris, M., Haddad, S., Saliari, M., Vasilakopoulou, K., Synnefa, A., Paolini, R., Ulpiani, G., Garshasbi, S., & Fiorito, F. (2018). On the energy impact of urban heat island in Sydney: Climate and energy potential of mitigation technologies. *Energy and Buildings*, 166, 154–164. <https://doi.org/10.1016/j.enbuild.2018.02.007>
- Santamouris, M., & Vasilakopoulou, K. (2023). Recent progress on urban heat mitigation technologies. *Science Talks*, 5, 100105. <https://doi.org/10.1016/j.sctalk.2022.100105>
- Santamouris, M. (2014). Cooling the cities—A review of reflective and green roof mitigation technologies to fight heat island and improve comfort in urban environments. *Solar Energy*, 103, 682–703. <https://doi.org/10.1016/j.solener.2012.07.003>. Scopus.
- Santamouris, M. (2020). Recent progress on urban overheating and heat island research. Integrated assessment of the energy, environmental, vulnerability and health impact. Synergies with the global climate change. *Energy and Buildings*, 207, 109482. <https://doi.org/10.1016/j.enbuild.2019.109482>
- Scherba, A., Sailor, D. J., Rosenstiel, T. N., & Wamser, C. C. (2011). Modeling impacts of roof reflectivity, integrated photovoltaic panels and green roof systems on sensible heat flux into the urban environment. *Building and Environment*, 46(12), 2542–2551. <https://doi.org/10.1016/j.buildenv.2011.06.012>
- Schwaab, J., Meier, R., Mussetti, G., Seneviratne, S., Bürgi, C., & Davin, E. L. (2021). The role of urban trees in reducing land surface temperatures in European cities. *Nature Communications*, 12(1), Article 1. <https://doi.org/10.1038/s41467-021-26768-w>
- Shafique, M., Kim, R., & Rafiq, M. (2018). Green roof benefits, opportunities and challenges – A review. *Renewable and Sustainable Energy Reviews*, 90, 757–773. <https://doi.org/10.1016/j.rser.2018.04.006>
- Sharma, A., Conry, P., Fernando, H. J. S., Hamlet, A. F., Hellmann, J. J., & Chen, F. (2016). Green and cool roofs to mitigate urban heat island effects in the Chicago metropolitan area: Evaluation with a regional climate model. *Environmental Research Letters*, 11(6), 064004. <https://doi.org/10.1088/1748-9326/11/6/064004>
- Su, M. A., Ngarambe, J., Santamouris, M., & Yun, G. Y. (2021). Empirical evidence on the impact of urban overheating on building cooling and heating energy consumption. *IScience*, 24(5), 102495. <https://doi.org/10.1016/j.isci.2021.102495>
- Synnefa, A., Karlessi, T., Gaitani, N., Santamouris, M., Assimakopoulos, D. N., & Papakatsikas, C. (2011). Experimental testing of cool colored thin layer asphalt and estimation of its potential to improve the urban microclimate. *Building and Environment*, 46(1), 38–44. Scopus. <https://doi.org/10.1016/j.buildenv.2010.06.014>
- Synthesis Report of the IPCC Sixth Assessment Report (AR6). Longer Report. (IPCC AR6 SYR). (2023). Intergovernmental Panel on Climate Change. https://www.ipcc.ch/report/ar6/syr/downloads/report/IPCC_AR6_SYR_LongerReport.pdf. Accessed 23 May 2023
- Taha, H. (2008). Episodic performance and sensitivity of the urbanized MM5 (uMM5) to perturbations in surface properties in Houston Texas. *Boundary-Layer Meteorology*, 127(2), 193–218. <https://doi.org/10.1007/s10546-007-9258-6>

- Takebayashi, H., & Moriyama, M. (2007). Surface heat budget on green roof and high reflection roof for mitigation of urban heat island. *Building and Environment*, 42(8), 2971–2979. <https://doi.org/10.1016/j.buildenv.2006.06.017>
- Taleghani, M., Sailor, D., & Ban-Weiss, G. A. (2016). Micrometeorological simulations to predict the impacts of heat mitigation strategies on pedestrian thermal comfort in a Los Angeles neighborhood. *Environmental Research Letters*, 11(2), 024003. <https://doi.org/10.1088/1748-9326/11/2/024003>
- Touchaei, A. G., Akbari, H., & Tessum, C. W. (2016). Effect of increasing urban albedo on meteorology and air quality of Montreal (Canada) – Episodic simulation of heat wave in 2005. *Atmospheric Environment*, 132, 188–206. <https://doi.org/10.1016/j.atmosenv.2016.02.033>
- United Nations. (2023, April 24). *India to overtake China as world's most populous country in April 2023, United Nations projects*. United Nations; United Nations. <https://www.un.org/en/desa/india-overtake-china-world-most-populous-country-april-2023-united-nations-projects>
- Vahmani, P., Sun, F., Hall, A., & Ban-Weiss, G. (2016). Investigating the climate impacts of urbanization and the potential for cool roofs to counter future climate change in Southern California. *Environmental Research Letters*, 11(12), 124027. <https://doi.org/10.1088/1748-9326/11/12/124027>
- Vijayaraghavan, K. (2016). Green roofs: A critical review on the role of components, benefits, limitations and trends. *Renewable and Sustainable Energy Reviews*, 57, 740–752. <https://doi.org/10.1016/j.rser.2015.12.119>
- Wang, Y., Berardi, U., & Akbari, H. (2016). Comparing the effects of urban heat island mitigation strategies for Toronto, Canada. *Energy and Buildings*, 114, 2–19. <https://doi.org/10.1016/j.enbuild.2015.06.046>
- Yang, J., Wang, Z.-H., Chen, F., Miao, S., Tewari, M., Voogt, J. A., & Myint, S. (2015). Enhancing hydrologic modelling in the coupled weather research and forecasting-urban modelling system. *Boundary-Layer Meteorology*, 155(1), 87–109. <https://doi.org/10.1007/s10546-014-9991-6>
- Yang, J., Mohan Kumar, D., & Ilamathy, Pyrgou, A., Chong, A., Santamouris, M., Kolokotsa, D., & Lee, S. E. (2018). Green and cool roofs' urban heat island mitigation potential in tropical climate. *Solar Energy*, 173, 597–609. <https://doi.org/10.1016/j.solener.2018.08.006>
- Yerramilli, A., Challa, V. S., Indracanti, J., Dasari, H., Baham, J., Patrick, C., Young, J., Hughes, R., White, L. D., Hardy, M. G., & Swanier, S. (2008). Some observational and modeling studies of the atmospheric boundary layer at Mississippi gulf coast for air pollution dispersion assessment. *International Journal of Environmental Research and Public Health*, 5(5), 484–497. <https://doi.org/10.3390/ijerph5050484>
- Zhang, N., Zhu, L., & Zhu, Y. (2011). Urban heat island and boundary layer structures under hot weather synoptic conditions: A case study of Suzhou City China. *Advances in Atmospheric Sciences*, 28(4), 855. <https://doi.org/10.1007/s00376-010-0040-1>
- Zhang, X., Huang, T., Gulakhmadov, A., Song, Y., Gu, X., Zeng, J., Huang, S., Nam, W.-H., Chen, N., & Niyogi, D. (2022). Deep learning-based 500 m spatio-temporally continuous air temperature generation by fusing multi-source data. *Remote Sensing*, 14(15), Article 15. <https://doi.org/10.3390/rs14153536>
- Zheng, Y., Alapaty, K., Herwehe, J. A., Genio, A. D. D., & Niyogi, D. (2016). Improving high-resolution weather forecasts using the Weather Research and Forecasting (WRF) model with an updated Kain-Fritsch Scheme. *Monthly Weather Review*, 144(3), 833–860. <https://doi.org/10.1175/MWR-D-15-0005.1>
- Zhou, Y., & Shepherd, J. M. (2010). Atlanta's urban heat island under extreme heat conditions and potential mitigation strategies. *Natural Hazards*, 52(3), 639–668. <https://doi.org/10.1007/s11069-009-9406-z>
- Zonato, A., Martilli, A., Gutierrez, E., Chen, F., He, C., Barlage, M., Zardi, D., & Giovannini, L. (2021). Exploring the effects of rooftop mitigation strategies on urban temperatures and energy consumption. *Journal of Geophysical Research: Atmospheres*, 126(21), e2021JD035002. <https://doi.org/10.1029/2021JD035002>

Publisher's Note

Springer Nature remains neutral with regard to jurisdictional claims in published maps and institutional affiliations.